Journal of Asian Earth Sciences 105 (2015) 338–359

Contents lists available at ScienceDirect

Journal of Asian Earth Sciences

journal homepage: www.elsevier.com/locate/jseaes

# Geochronological, geochemical and Nd–Hf isotopic constraints on the petrogenesis of Late Cretaceous A-type granites from the southeastern coast of Fujian Province, South China

Jiao-Long Zhao [a,1], Jian-Sheng Qiu [a,*], Liang Liu [a,b,1], Rui-Qiang Wang [a,1]

[a] State Key Laboratory for Mineral Deposits Research, School of Earth Sciences and Engineering, Nanjing University, Nanjing 210023, China
[b] State Key Laboratory of Ore Deposit Geochemistry, Institute of Geochemistry, Chinese Academy of Sciences, Guiyang 550002, China

ARTICLE INFO

*Article history:*
Received 14 October 2014
Received in revised form 22 January 2015
Accepted 23 January 2015
Available online 3 February 2015

*Keywords:*
Aluminous A-type granites
Zircon U–Pb ages
Geochemistry
Petrogenesis
Southeastern coast of Fujian Province, South China

ABSTRACT

We present comprehensive petrological, geochronological, major and trace element, and Nd–Hf isotopic data for the Baishishan, Jingangshan, and Wushan granitic plutons on the southeastern coast of Fujian Province, South China, with the aims of elucidating their origin and gaining new insights into the petrogenesis of aluminous A-type granites. Zircon U–Pb ages obtained by laser ablation–inductively coupled plasma–mass spectrometry show that the three investigated plutons were emplaced at 92–86 Ma, indicating that they were generated during a Late Cretaceous magmatic event. The granites from the three plutons are composed mainly of perthite, quartz, plagioclase, and minor biotite; they have high $SiO_2$ contents, and low CaO, MnO, $Fe_2O_3^{tot}$, and MgO contents, and show a metaluminous to slightly peraluminous signature. The granites are enriched in some large ion lithophile elements (e.g., Rb, Th, and U) and high field strength elements (e.g., Nb and Ta) with elevated Ga/Al ratios, and spidergrams show strong depletions in Ba, Sr, Ti, and P. Chondrite-normalized REE patterns show relative enrichments in light rare earth elements, flat heavy rare earth element profiles, and strongly negative Eu anomalies. These mineralogical and geochemical characteristics suggest that all three plutons can be classified as aluminous A-type granites. The plutons exhibit nearly identical whole-rock Nd and zircon Hf isotopic compositions, and yield Mesoproterozoic two-stage model ages (1.4–1.1 Ga) for both Nd and Hf isotopes. Based on a synthesis of the geochemical and isotopic data and petrogenetic modelling, we suggest that these A-type granitic rocks were most likely formed by variable degrees of fractional crystallization of magmas produced by the partial melting of a tonalitic to granodioritic source, with plagioclase-rich residual phases in the middle to lower crust, and emplaced at shallow crustal levels along the Changle–Nan'ao Fault. Our data on the Baishishan, Jingangshan, and Wushan granites, coupled with previous studies of Cretaceous magmatism in coastal areas of SE China, indicate that a gradually intensifying regional extension took place in the region during the late Yanshanian (Cretaceous), which peaked during the Late Cretaceous in response to the roll-back of the Palaeo-Pacific plate. Consequently, we conclude that the generation of A-type granites was related to intensive tectonic extension along the Changle–Nan'ao Fault and the induced underplating of mantle-derived magma.



## 1. Introduction

A-type granites have attracted much research attention in recent decades because of their unusual mineralogical and chemical characteristics and their potential value for reconstructing the tectonic settings of ancient terranes. High Ga/Al ratios and enrichments in alkali and high field strength elements (HFSEs) are regarded as being diagnostic of A-type granitoids (Eby, 1990; Nardi and Bitencourt, 2009; Whalen et al., 1987). An important characteristic of A-type magmas is that they generally occur in extension-related tectonic settings, ranging from post-orogenic to anorogenic (Bonin, 2007; Eby, 1990, 1992). Such granitoids have long been recognized as being peraluminous to peralkaline in composition (Collins et al., 1982; Creaser et al., 1991; Eby, 1990; Karsli et al., 2012; Mushkin et al., 2003; Poitrasson et al., 1994, 1995; Whalen et al., 1987), and King et al. (1997) first proposed that they can be further divided into aluminous and peralkaline subgroups.

* Corresponding author. Tel.: +86 25 89686824; fax: +86 25 83686016.
*E-mail addresses:* jlz2007@yeah.net (J.-L. Zhao), jsqiu@nju.edu.cn (J.-S. Qiu), liuliang0830@126.com (L. Liu), vickwrq2008@163.com (R.-Q. Wang).
[1] Tel.: +86 25 89686824; fax: +86 25 83686016.

http://dx.doi.org/10.1016/j.jseaes.2015.01.022
1367-9120/

In contrast to the peralkaline A-type granites, the aluminous A-type granites are metaluminous to slightly peraluminous, commonly show higher $Al_2O_3$ abundances, lower alkali, HFSE and REE contents, and lower $FeO^{tot}$/MgO and Ga/Al ratios, and they commonly contain Al-rich minerals such as spessartine and Mn-rich muscovite (King et al., 1997, 2001; Wu et al., 2002; Qiu et al., 2004). Previous studies have proposed several models to elucidate the genesis of the aluminous A-type granites. For example, Collins et al. (1982) suggested that the metaluminous to peraluminous A-type granites from the Lachlan Fold Belt, now considered to belong to the aluminous sub-group, were generated through the partial melting of a residual source after the extraction of I-type magmas. Farahat et al. (2007) advocated that aluminous A-type granites from the Eastern Desert of Egypt were derived from the dehydration melting of tonalitic to granodioritic sources. In southwestern Corsica, France, the aluminous A-type granites appear to have been generated through the partial melting of amphibole-bearing and $K_2O$-rich mafic cumulates which had not experienced any previous partial melting (Poitrasson et al., 1994, 1995). The generation of Hercynian post-collisional granitoids in southern Tien Shan, Kyrgyzstan, was thought to have involved crust–mantle interactions (Konopelko et al., 2007). Li et al. (2007) considered that some aluminous A-type granites had likely been produced by extreme fractionation of a mantle-derived alkaline parental magma, coupled with crustal assimilation. Rajesh (2000) reported that the Pan-African Ambalavayal granite was generated by the partial melting of a charnockitic source. Evidently, the formation of aluminous A-type granites may involve multiple processes,

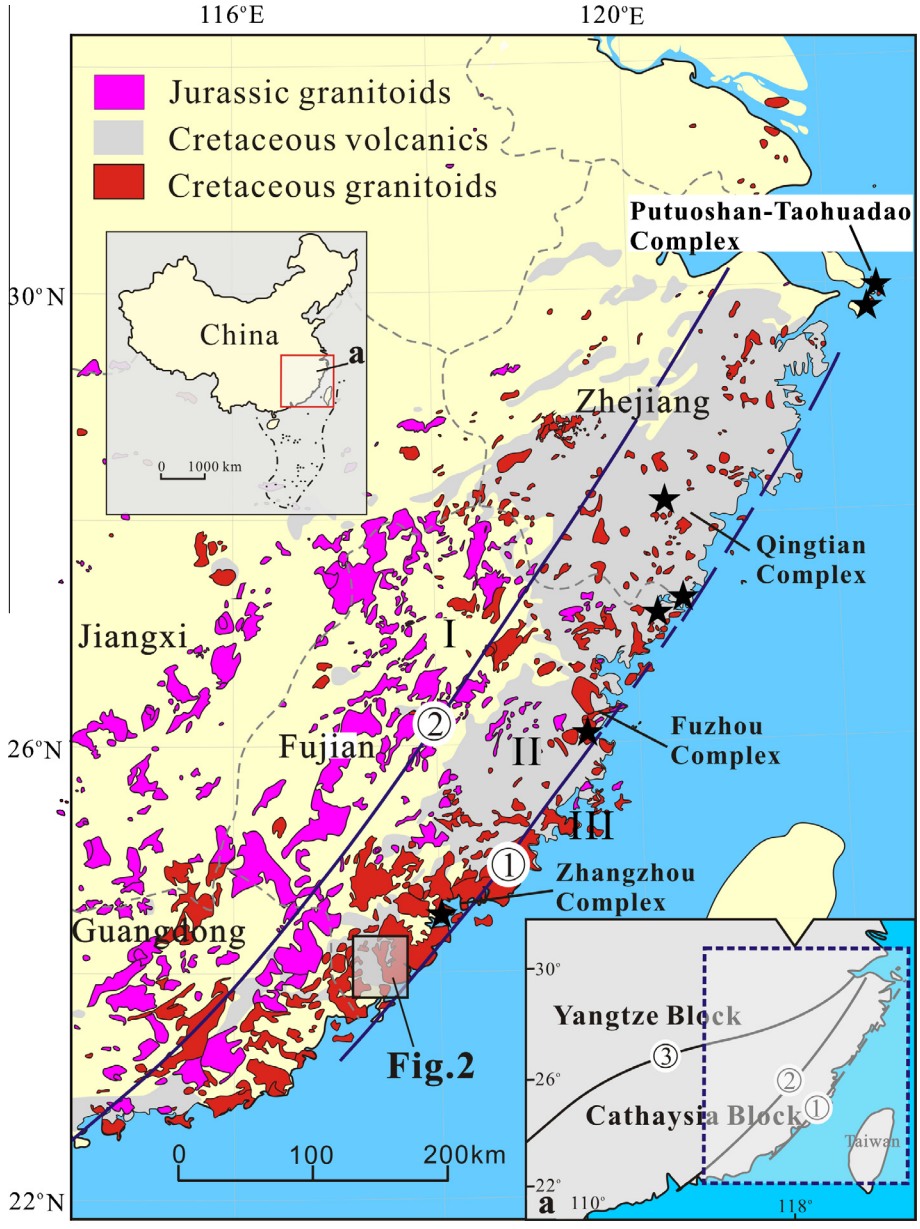


**Fig. 1.** Schematic map showing the distribution of the Yanshanian granitoids and volcanic rocks in SE China, and the location of the study area (modified after Zhou et al., 2006). The localities of representative A-type granites in the coastal area are marked with black stars. Names of the fault zones: ① – Changle–Nan'ao fault; ② – Zhenghe–Dapu fault; ③ – Jiangshan–Shaoxing fault. Major tectonic belts: I – the Early Palaeozoic fold belt; II – the Yanshanian magmatic belt; III – the Pingtan–Dongshan metamorphic belt.

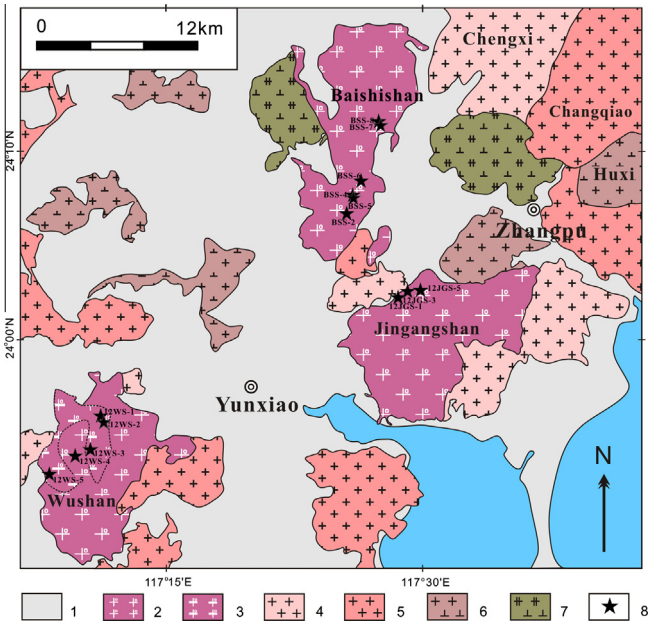


**Fig. 2.** Simplified geological map of the southern region of Zhangzhou, coastal Fujian Province (modified after the 1:200,000 geological map of Zhangzhou and Dongshan Sheets). 1 – Yanshanian volcanic-sedimentary rocks; 2 – miarolitic alkali feldspar granite; 3 – porphyritic miarolitic alkali feldspar granite; 4 – alkali feldspar granite; 5 – biotite granite; 6 – granodiorite; 7 – quartz diorite; 8 – sampling location.

and the magmas can be generated in diverse geological settings; thus, their petrogenesis is still a subject of considerable controversy.

A-type granites in the coastal area of SE China are generally distributed along a NNE-trending belt subparallel to the Changle–Nan'ao Fault, approximately 800 km long and 60–80 km wide (Fig. 1). They can be further divided into two subgroups, aluminous A-types (AA types) and peralkaline A-types (PA types), according to their mineralogical and geochemical characteristics. The majority of the A-type granites in this belt are alkali feldspar granites of the AA type, and PA granites are relatively rare. These A-type granites are temporally and spatially associated with widespread I-type granitoids, forming characteristic I- and A-type composite granitic plutons, such as the Zhangzhou, Fuzhou, Qingtian, and Putuoshan–Taohuadao complexes (Fig. 1). Previous studies have provided mineralogical, geochemical, and whole-rock Sr–Nd isotopic constraints on the petrogenesis and evolution of the A-type granites in SE China coastal areas (Hong et al., 1987; Martin et al., 1994; Qiu et al., 2004; Zhou and Wu, 1994). However, their petrogenesis is a matter of debate; in particular, their source characteristics and the geodynamic mechanisms responsible for their generation are poorly constrained. In this paper, we report new, high-precision zircon U–Pb ages, in situ zircon Hf isotopic compositions, and whole-rock elemental and Nd isotope data for three representative aluminous A-type plutons (the Baishishan, Jingangshan, and Wushan plutons) (Fig. 2) located in the coastal area of southeastern Fujian Province. The aims of the study are to identify the nature of magma sources, to elucidate their petrogenesis, and to develop a tectonomagmatic model for the origin and evolution of the A-type and associated I-type granitoids.

## 2. Geological background

The South China Block, located on the eastern margin of Eurasia, is surrounded by the Qinling–Dabie orogenic belt to the north, the Tibetan Block to the west, and the Indochina Block to the south. It is composed of two major Precambrian continental blocks: the Yangtze Block in the northwest and the Cathaysia Block in the southeast, separated by the Jiangshan–Shaoxing suture zone (Fig. 1, lower right inset; Chen and Jahn, 1998; Zhang and Wang, 2007). Mesozoic volcanic–intrusive magmatism was largely concentrated in the Cathaysia Block, and the intensity of magmatism increased toward the ocean (Zhou et al., 2006). Two major NNE–SSW-trending trans-lithospheric faults in the eastern Cathaysia Block (i.e., the Zhenghe–Dapu and Changle–Nan'ao faults) separate the region into three main tectonic belts, which from west to east are the early Palaeozoic fold belt, the Yanshanian magmatic belt, and the Pingtan–Dongshan metamorphic belt (Fig. 1; Zhao et al., 2004, 2007). The early Palaeozoic fold belt, located northwest of the Zhenghe–Dapu Fault, is characterized by abundant exposures of Precambrian basement rocks, which comprise the Palaeoproterozoic Mayuan (amphibolite facies) and Neoproterozoic Mamianshan (upper-greenschist to lower-amphibolite facies) groups (Li, 1997; Li et al., 2005). The belt was strongly overprinted by widespread late Mesozoic magmatism and local Caledonian and Indosinian events (Xu et al., 2007). The Yanshanian magmatic belt is made up of Cretaceous granitoids and equivalent volcanic rocks, as well as some Jurassic granites. The granitic rock assemblages in the belt are predominantly high-K calc-alkaline I-type granitoids ranging from tonalites to alkali feldspar granites, and succeeding shallow-level A-type granites (Hong et al., 1987; Martin et al., 1994; Qiu et al., 1999a). Overall, the granitoids with Early Yanshanian (Jurassic) ages are mainly distributed in the Cathaysia interior and those with the Late Yanshanian (Cretaceous) ages are concentrated in the southeastern coastal area (Fig. 1). The Pingtan–Dongshan metamorphic belt occurs along the coastal area of Fujian Province, including Pingtan Island, Mazu Island, the Jinjiang area, and Dongshan Island. Exposed rocks in the metamorphic belt include Yanshanian regionally metamorphosed rocks, Mesozoic granites, volcanic rocks, and minor mafic rocks (Chen et al., 2002, 2004; Shu et al., 2000; Yang et al., 2010).

As products of Cretaceous magmatism, the Baishishan, Jingangshan, and Wushan granitic plutons in the coastal area of Fujian Province were emplaced roughly along the Changle–Nan'ao shear zone (Fig. 1). These plutons intruded into Early Cretaceous volcanic–sedimentary rocks of the Shimaoshan Group and Late Jurassic low-grade metasedimentary rocks of the Douling Group, as well as into some early granitoids. No chilled margins are observed in the plutons. Field observations and existing zircon U–Pb ages indicate that the three plutons are spatially and temporally associated with the Zhangpu I-type composite granite pluton (Fig. 2), which is composed of the Changqiao (CQ) biotite granite (119 Ma), the Chengxi (CX) alkali feldspar granite (101 Ma), and the Huxi (HX) granodiorite (96 Ma). This I-type composite granite pluton is thought to have been derived from the mixing of juvenile mantle- and crust-derived magmas (Qiu et al., 2012).

## 3. Petrography

The Baishishan pluton, located in the western part of Zhangpu County, southeastern Fujian Province, has an outcrop area of ~180 km$^2$ (Fig. 2). This pluton is lithologically homogeneous and consists mainly of medium-grained alkali feldspar granite and subordinate granite. The major mineral phases are perthite (45–55 vol.%), quartz (25–35 vol.%), and plagioclase (An = 15–30, 10–15 vol.%), with less than 3 vol.% biotite. Accessory minerals are magnetite, titanite, apatite, zircon, and allanite. Biotite crystals are euhedral to subhedral, strongly pleochroic, and contain abundant fine-grained inclusions of zircon that form pleochroic haloes. Both perthite, which locally contains small euhedral to subhedral inclusions of plagioclase crystals, and quartz occur as interstitial

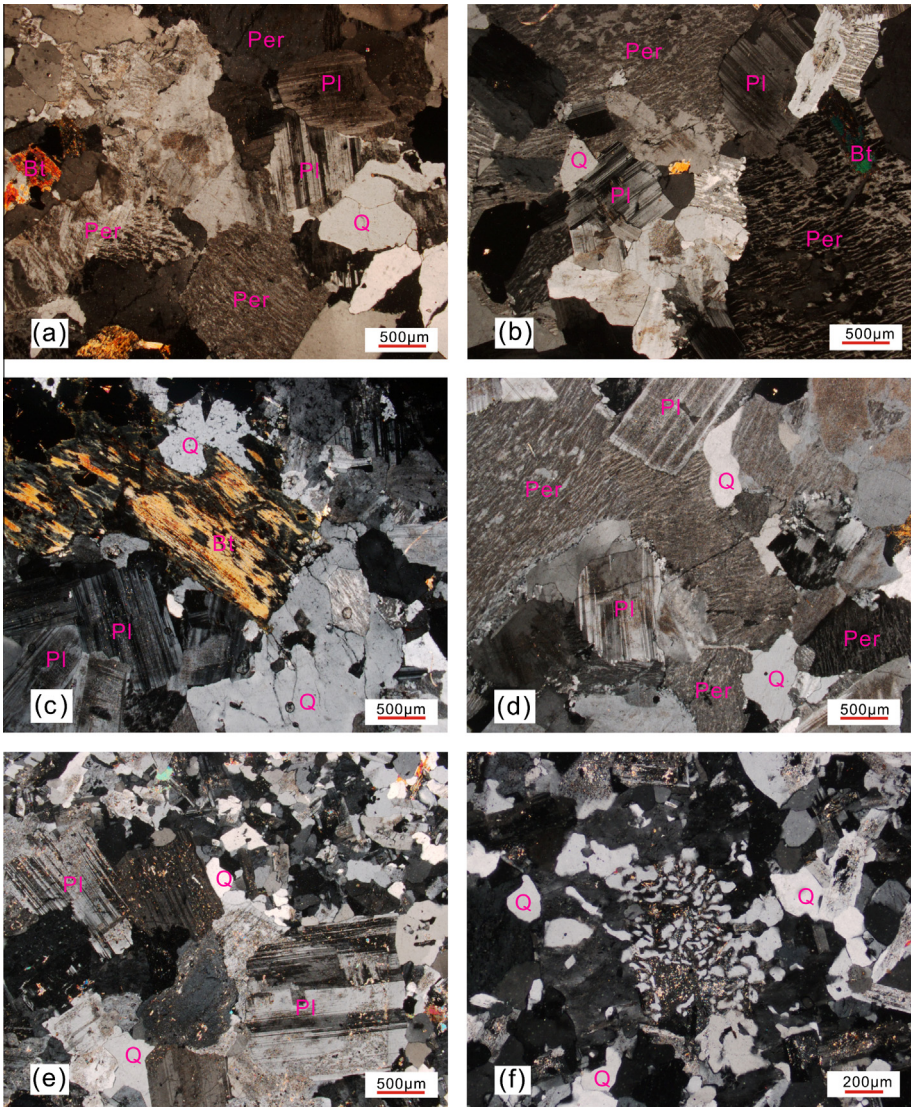


**Fig. 3.** Microphotographs of representative samples from Baishishan (a, b), Jingangshan (c, d) and Wushan (e, f) plutons. All the photos were taken under crossed nicols. Mineral abbreviation: Q – quartz; Per – perthite; Pl – plagioclase; Bt – biotite.

phases (Fig. 3a and b). Miarolitic cavities and granophyric texture are fairly common.

The Jingangshan pluton, which is located to the south of the Baishishan pluton, has an outcrop area of 165 km$^2$ (Fig. 2). The granites are faint red to ashen in color, and massive with a medium-grained granitic texture. They are composed of perthite (45–55 vol.%), quartz (25–35 vol.%), plagioclase (An = 20–30, 10–15 vol.%), and biotite (<3 vol.%), with minor amounts of magnetite, zircon, apatite, and titanite. The mineral composition is typical of alkali feldspar granite. Biotite occurs as isolated subhedral to euhedral crystals (Fig. 3c). Plagioclase occurs as euhedral laths with well-developed polysynthetic twinning, and lacks oscillatory zoning (Fig. 3d). Miarolitic cavities and micrographic intergrowths of quartz and perthite are also well developed, as in the Baishishan pluton, and mafic microgranular enclaves are rarely observed.

The Wushan pluton, which is located on the border between Yunxiao and Zhao'an counties in southwestern Fujian Province, is exposed as a N–S-trending spindle-shaped batholith with an outcrop area of 145 km$^2$ (Fig. 2). Unlike the Baishishan and Jingangshan plutons, the Wushan pluton exhibits obvious lithological zoning, and consists mainly of alkali feldspar granite in the central facies and porphyritic alkali feldspar granite in the marginal facies (Fig. 2). The texture varies from porphyritic in the marginal facies (Fig. 3e) to medium-grained equigranular in the central facies, but otherwise, they have similar mineral assemblages. The granites of the central facies are light gray to reddish in color, and are composed mainly of perthite (50–55 vol.%), quartz (30–35 vol.%), plagioclase (An = 20–28, 10–15 vol.%), and biotite (<3 vol.%). The granites of the marginal facies are light pink and contain phenocrysts of perthite (3–12 mm), quartz (2–5 mm), and minor plagioclase (1.5–2 mm); their groundmasses display micrographic textures (Fig. 3f) and consist mainly of fine-grained perthite, quartz, and plagioclase, with minor biotite, zircon, and titanite. As in the Jingangshan and Baishishan plutons, mafic enclaves are absent and miarolitic cavities are well developed.

Overall, the mineral assemblages and lithological features of all three plutons are similar. In contrast to spatially coexisting Zhangpu I-type granites, the granophyric textures and miarolitic cavities of the A-type granite plutons are much more well developed, suggesting shallower depth of emplacement (Hergt et al., 2007; Mushkin et al., 2003). Moreover, some aluminous-rich minerals (such as spessartine, muscovite, etc.) have been found in

these plutons, especially in their miarolitic cavities (Hong et al., 1987; Qiu et al., 2004).

## 4. Sampling and analytical methods

### 4.1. Zircon U–Pb dating and Hf isotopes

Zircons from five samples (BSS-4 and BSS-8 from the Baishishan pluton, 12JGS-5 from the Jingangshan pluton, and 12WS-1 and 12WS-4 from the Wushan pluton) were separated by conventional techniques, including crushing, sieving, and magnetic and heavy liquid separation methods. Zircon grains, handpicked under a binocular stereomicroscope, were mounted in epoxy resin, and then polished to expose their centres. Cathodoluminescence (CL) and optical microscopy images were taken to ensure that the least fractured and most inclusion-free zones of the zircons were analyzed. The CL images were obtained using a Mono CL3+(Gatan, Pleasanton, CA, USA) attached to a scanning electron microscope (Quanta 400 FEG, Hillsboro, OR, USA) at the State Key Laboratory of Continental Dynamics, Northwest University, Xi'an, China.

Zircon U–Pb isotopic analyses were performed using an Agilent 7500a inductively coupled plasma–mass spectrometer (ICP–MS) coupled to a New Wave Research 213-nm laser ablation system at the State Key Laboratory for Mineral Deposits Research, Nanjing University. The ablated material was transported in a He carrier gas through PVC tubing (inner diameter, 3 mm) and combined with argon in a 30-$cm^3$ mixing chamber prior to entry into the ICP–MS. Analyses were conducted using a beam diameter of 25 μm, a repetition rate of 5 Hz, and an energy of 10–20 $J/cm^2$. Data acquisition for each analysis took 100 s (40 s on the background signal and 60 s on the ablated signal). A homogeneous standard zircon (GEMOC GJ-1: $^{207}Pb/^{206}Pb$ age of 608.5 ± 0.4 Ma and a relatively young $^{206}Pb/^{238}U$ age of 599.8 ± 4.5 Ma; Jackson et al., 2004) was used to correct the mass discrimination of the MS and the residual elemental fractionation. A well-characterized zircon standard (Mud Tank; intercept age, 732 ± 5 Ma; Black and Gulson, 1978) was used as an independent control on reproducibility and instrument stability. The raw ICP–MS U–Pb isotopic data were acquired using GLITTER 4.4, using the correction method for common Pb described by Andersen (2002). Mean age calculations and Concordia diagram plots were performed using Isoplot (version 2.49) (Luding, 2001).

In situ zircon Hf isotope analyses were performed using a Thermo Scientific Neptune Plus multi-collector (MC) ICP–MS attached to a New Wave UP193 solid-state laser ablation system at the State Key Laboratory for Mineral Deposits Research, Nanjing University. Zircons were ablated with a beam diameter of 35 μm, energy of 11.24–11.65 $J/cm^2$, 8-Hz laser repetition rate, and a 26-s laser ablation time. Two reference standards were also measured to evaluate the reliability of the data (Mud Tank $^{176}Hf/^{177}Hf$ ratio = 0.282493 ± 0.000011, $n$ = 13, 2$\sigma$ and Penglai $^{176}Hf/^{177}Hf$ ratio = 0.282898 ± 0.000019, $n$ = 11, 2$\sigma$) before the analyses of unknown samples. The measured $^{176}Hf/^{177}Hf$ ratios of the two standards agree with recommended values within 2$\sigma$ errors (Griffin et al., 2007; Li et al., 2010).

### 4.2. Whole-rock major elements, trace elements, and Nd isotopes

All samples selected for chemical and isotopic analyses were fresh, and were crushed and powdered to 200 mesh using an agate mill. Whole-rock major elements, trace elements, and Nd isotopic compositions were determined at the State key Laboratory for Mineral Deposits Research, Nanjing University, China. For major element analyses, mixtures of whole-rock powders (0.5 g) and $Li_2B_4O_7$ + $LiBO_2$ + LiBr (11 g) were made into glass discs and then analyzed using a Thermo Scientific ARL 9900 X-ray fluorescence (XRF) spectrometer. The analytical precision was estimated to be less than 10% for all major elements and less than 1% for the majority of elements. For trace element analyses, ~50 mg of powder was dissolved in high-pressure Teflon bombs using a HF + $HNO_3$ mixture; Rh was used as an internal standard to monitor for signal drift during the ICP–MS analyses. Trace element concentrations were determined using a Finnigan Element II ICP–MS. Detailed analytical procedures followed Gao et al. (2003). The analytical precision was better than 10% for all trace elements, with the majority being better than 5%.

For whole-rock Nd isotope analyses, ~50 mg of powder was dissolved in Teflon beakers with a HF + $HNO_3$ mixture, and Nd was then separated and purified using a cation-exchange resin with HIBA as the eluent. The detailed chemical separation and isotopic measurement procedures used are described in Pu et al. (2004, 2005). The isotopic compositions of the purified Nd solutions were determined on a Thermo Scientific Neptune Plus MC–ICP–MS. For the present analyses, the Nd isotopic ratios were corrected for mass fractionation by normalizing to $^{146}Nd/^{144}Nd$ = 0.7219. During the analysis period, measurements of the Japan JNdi-1 Nd standard yielded a $^{143}Nd/^{144}Nd$ ratio of 0.512096 ± 0.000008 ($n$ = 18, 2$\sigma$).

## 5. Analytical results

### 5.1. Zircon U–Pb dating

The CL images of representative zircons are shown in Fig. 4. The results of LA–ICP–MS U–Pb isotopic analyses are listed in Table 1, and are presented graphically in Fig. 5. Because low $^{207}Pb$ count rates result in large statistical uncertainties, the measured $^{206}Pb/^{238}U$ ages are considered to be more precise for younger zircons (<1 Ga), and the $^{207}Pb/^{206}Pb$ ages are considered to be more precise for older zircons (>1 Ga). Therefore, we used the $^{206}Pb/^{238}U$ data to represent the crystallization ages of Phanerozoic zircons. The age results for the five samples from the three plutons are discussed in turn below.

#### 5.1.1. Baishishan pluton

Zircons of two samples from the Baishishan pluton were selected for analysis, BSS-4 in the south and BSS-8 in the north (Fig. 2). Most zircons are pale-yellow, transparent, euhedral, and prismatic grains with well-developed magmatic oscillatory zoning and sector zonation in CL images (Fig. 4); their lengths range from 50 to 100 μm and their length to width ratios from 1:1 to 2:1. No core–rim textures are observed (Fig. 4). They have high and variable uranium (440–1485 ppm, 471–2028 ppm) and thorium (601–2402 ppm, 426–2529 ppm) concentrations, with Th/U ratios of 0.94–2.47 and 1.12–2.28, respectively, indicating a magmatic origin. Twelve analyses for BSS-4 and seventeen analyses for BSS-8 were performed, with all ages being concordant or nearly concordant, yielding weighted mean $^{206}Pb/^{238}U$ ages of 91.0 ± 1.0 Ma (2$\sigma$, MSWD = 1.4, Fig. 5a) and 91.7 ± 0.7 Ma (2$\sigma$, MSWD = 1.4, Fig. 5b). As the two ages are consistent within analytical error, we consider that the Baishishan pluton crystallized at 91 Ma.

#### 5.1.2. Jingangshan pluton

Zircons from the sample 12JGS-5 are mostly transparent, colorless to light yellow, and euhedral, with concentric zoning under CL. The zircons are up to 50–100 μm long, have length to width ratios of 2:1, and show high but variable contents of U (95–2713 ppm) and Th (253–4421 ppm), with Th/U ratios ranging from 1.31 to 2.72. Seventeen analyses were carried out, and all results plot on or near the Concordia curve, yielding a weighted mean $^{206}Pb/^{238}U$ age of 86.2 ± 0.6 Ma (2$\sigma$, MSWD = 0.54; Fig. 5c), which

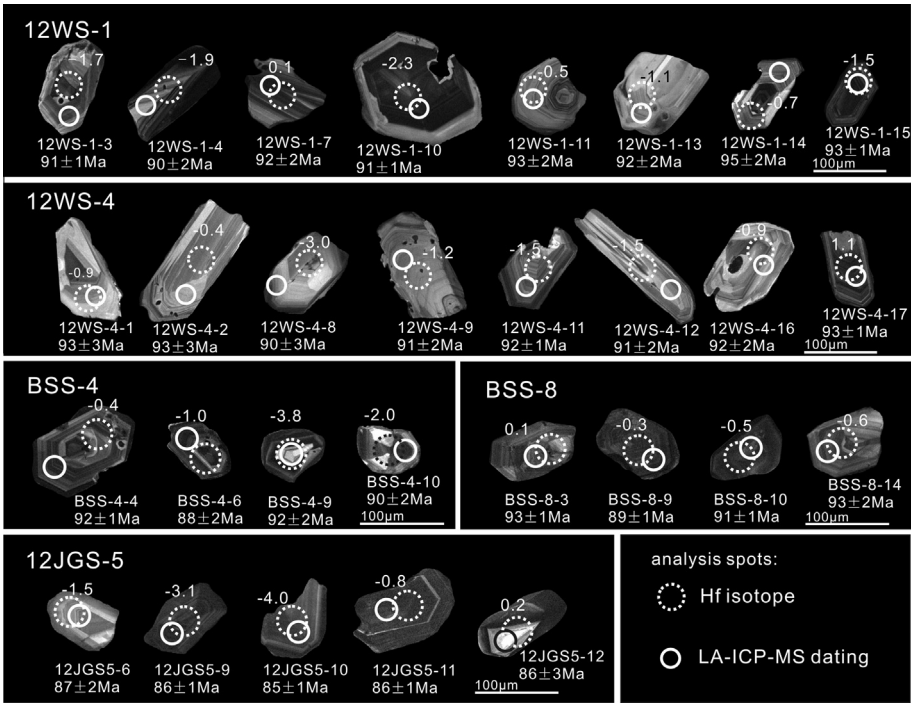


**Fig. 4.** CL images of representative zircons from granites of Baishishan, Jingangshan and Wushan plutons. The $^{206}Pb/^{238}U$ ages and $\varepsilon_{Hf}(t)$ values are shown.

is considered to be the crystallization age of the Jingangshan pluton.

*5.1.3. Wushan pluton*

Sample 12WS-1, which was collected from the northern part of the Wushan pluton, belongs lithologically to the marginal facies. Zircons from this sample are transparent, colorless to light yellow, pyramidal or prismatic, up to 50–120 μm in length, and have length to width ratios of 1:1 to 2:1. Sample 12WS-4, which was collected from the central part of the pluton, belongs to the central facies. Zircon grains from this sample are coarser, up to 80–200 μm in length, have length to width ratios varying from 1:1 to 4:1, and have other characteristics similar to those of 12WS-1. The zircon grain-size trends, combined with the petrographic observations, indicate that rocks from the central facies experienced slower cooling rates than rocks from the marginal facies. All zircon grains show typical magmatic oscillatory zoning in CL images, no inherited cores (Fig. 4), and Th/U ratios greater than 0.4, suggesting a magmatic origin. Eighteen and nineteen analyses were performed on samples 12WS-1 and 12WS-4, respectively. The results of all analyses are concordant or nearly concordant, yielding weighted mean $^{206}Pb/^{238}U$ ages of 92.0 ± 0.6 Ma ($2\sigma$, MSWD = 1.0; Fig. 5d) and 92.1 ± 0.6 Ma ($2\sigma$, MSWD = 1.1; Fig. 5e), respectively. The two ages are consistent within analytical uncertainties, and therefore we consider that the age of 92 Ma represents the crystallization age of the Wushan pluton.

*5.2. Major and trace elements*

Results of the analyses of 14 samples selected for determinations of major and trace element compositions are presented in Table 2. As all of the samples show similar geochemical features, we describe them collectively.

All of the analyzed samples are strongly siliceous, with a high and restricted range of $SiO_2$ contents (75.18–78.79 wt.%); this is also reflected in their high differentiation index values (D.I. > 94; Table 2). The samples also have relatively high alkali contents, with $K_2O + Na_2O$ values of 7.72–8.92 wt.% and $K_2O/Na_2O$ ratios of 0.9–1.2, and they fall within the alkaline field on an $SiO_2$–alkalinity ratio (A.R.) diagram (Fig. 6a). All the granites are classified as high-K calc-alkaline rocks according to the $K_2O$ *vs.* $SiO_2$ classification scheme (Fig. 6b). They have moderate $Al_2O_3$ contents, ranging from 11.56 to 12.92 wt.%, with A/CNK ratios generally around 1.0. On an A/CNK–A/NK plot (Fig. 6c), nearly all the samples fall in the metaluminous or weakly peraluminous fields. According to the classification scheme for granitoids proposed by Frost et al. (2001), these granites exhibit a ferroan signature, with $FeO^{tot}/(FeO^{tot} + MgO)$ ranging from 0.83 to 0.92, and fall into the A-type granite field (Fig. 6d). In addition, all of the rocks are characterized by low CaO (0.22–0.81 wt.%), MgO (0.06–0.17 wt.%), $Fe_2O_3^{tot}$ (0.63–1.14 wt.%), MnO (0.04–0.13 wt.%), and $P_2O_5$ (0.01–0.04 wt.%) values, even in the samples from the marginal facies of the Wushan pluton.

The samples from the Baishishan, Jingangshan, and Wushan plutons have total rare earth element abundances (ΣREEs) of 86.9–136.6 ppm, 92.4–253.5 ppm, and 84.7–128.4 ppm, respectively. In the chondrite-normalized REE patterns, these granites show slight enrichment of light rare earth elements (LREEs) relative to heavy rare earth elements (HREEs) [$(La/Yb)_N$ = 3.9–13.1], nearly flat HREE distributions [$(Gd/Yb)_N$ = 0.3–1.4], and significant negative Eu anomalies ($Eu/Eu^*$ = 0.11–0.52; Fig. 7a, c, and e), especially in the Baishishan granites, which are similar to those reported for A-type granites (Dahlquist et al., 2010; Konopelko et al., 2007). A noteworthy feature of all the samples is their roughly similar REE patterns, suggesting that they have similar magma source. Moreover, all of the samples are characterized by obvious enrichments in large ion lithophile elements (LILEs; e.g., Rb, Cs, K, Th, and U), high field strength elements (HFSEs; e.g., Ta and Nb), and strong depletion of Ba, Sr, Ti, and P (Fig. 7b, d, and f), which agrees with the element compositional patterns of A-type granites (Whalen et al., 1987; Wu et al., 2002). In the Wushan pluton, trace element concentrations exhibit a wide range of variation

**Table 1**
LA–ICP–MS zircon U–Pb dating results of representative samples from the Baishishan, Jingangshan and Wushan plutons.

| Spot no. | Th/U | Isotopic ratios | | | | | | Ages (Ma) | | | |
|---|---|---|---|---|---|---|---|---|---|---|---|
| | | $^{207}Pb/^{206}Pb$ | | $^{207}Pb/^{235}U$ | | $^{206}Pb/^{238}U$ | | $^{207}Pb/^{235}U$ | | $^{206}Pb/^{238}U$ | |
| | | Ratios | ±1σ | Ratios | ±1σ | Ratios | ±1σ | Age | ±1σ | Age | ±1σ |
| *Baishishan pluton* | | | | | | | | | | | |
| BSS-4, coordinate: N24°07′45.4″, E117°26′05.0″ | | | | | | | | | | | |
| BSS4-01 | 1.87 | 0.05319 | 0.00184 | 0.10201 | 0.00342 | 0.01392 | 0.00024 | 99 | 3 | 89 | 2 |
| BSS4-02 | 1.81 | 0.05673 | 0.00239 | 0.10858 | 0.00436 | 0.01390 | 0.00028 | 105 | 4 | 89 | 2 |
| BSS4-03 | 1.58 | 0.06069 | 0.00169 | 0.11654 | 0.00311 | 0.01393 | 0.00022 | 112 | 3 | 89 | 1 |
| BSS4-04 | 1.26 | 0.04786 | 0.00077 | 0.09465 | 0.00150 | 0.01434 | 0.00020 | 92 | 1 | 92 | 1 |
| BSS4-05 | 0.94 | 0.05644 | 0.00143 | 0.11110 | 0.00273 | 0.01428 | 0.00022 | 107 | 2 | 91 | 1 |
| BSS4-06 | 1.31 | 0.05254 | 0.00188 | 0.09935 | 0.00340 | 0.01373 | 0.00025 | 96 | 3 | 88 | 2 |
| BSS4-07 | 1.73 | 0.04796 | 0.00079 | 0.09364 | 0.00154 | 0.01416 | 0.00021 | 91 | 1 | 91 | 1 |
| BSS4-08 | 1.27 | 0.05152 | 0.00188 | 0.10337 | 0.00364 | 0.01456 | 0.00025 | 100 | 3 | 93 | 2 |
| BSS4-09 | 2.43 | 0.04688 | 0.00216 | 0.09255 | 0.00416 | 0.01432 | 0.00025 | 90 | 4 | 92 | 2 |
| BSS4-10 | 2.47 | 0.04888 | 0.00163 | 0.09485 | 0.00300 | 0.01406 | 0.00026 | 92 | 3 | 90 | 2 |
| BSS4-11 | 1.51 | 0.04778 | 0.00086 | 0.09561 | 0.00169 | 0.01451 | 0.00022 | 93 | 2 | 93 | 1 |
| BSS4-12 | 1.44 | 0.04610 | 0.00135 | 0.09206 | 0.00261 | 0.01449 | 0.00024 | 89 | 2 | 93 | 2 |
| BSS-8, coordinate: N24°11′39.4″, E117°27′35.7″ | | | | | | | | | | | |
| BSS8-01 | 1.41 | 0.04854 | 0.00138 | 0.09419 | 0.00259 | 0.01410 | 0.00024 | 91 | 2 | 90 | 2 |
| BSS8-02 | 1.25 | 0.04852 | 0.00114 | 0.09609 | 0.00220 | 0.01437 | 0.00023 | 93 | 2 | 92 | 1 |
| BSS8-03 | 1.15 | 0.04815 | 0.00091 | 0.09628 | 0.00181 | 0.01450 | 0.00021 | 93 | 2 | 93 | 1 |
| BSS8-04 | 1.20 | 0.04814 | 0.00305 | 0.09549 | 0.00585 | 0.01440 | 0.00032 | 93 | 5 | 92 | 2 |
| BSS8-05 | 1.62 | 0.04910 | 0.00068 | 0.09638 | 0.00134 | 0.01424 | 0.00019 | 93 | 1 | 91 | 1 |
| BSS8-06 | 1.28 | 0.05138 | 0.00110 | 0.10214 | 0.00215 | 0.01443 | 0.00022 | 99 | 2 | 92 | 1 |
| BSS8-07 | 1.68 | 0.04828 | 0.00086 | 0.09539 | 0.00170 | 0.01434 | 0.00021 | 93 | 2 | 92 | 1 |
| BSS8-08 | 1.18 | 0.04814 | 0.00126 | 0.09739 | 0.00251 | 0.01468 | 0.00023 | 94 | 2 | 94 | 1 |
| BSS8-09 | 1.35 | 0.04949 | 0.00081 | 0.09488 | 0.00154 | 0.01391 | 0.00020 | 92 | 1 | 89 | 1 |
| BSS8-10 | 1.60 | 0.05015 | 0.00125 | 0.09869 | 0.00239 | 0.01427 | 0.00021 | 96 | 2 | 91 | 1 |
| BSS8-11 | 1.12 | 0.04828 | 0.00169 | 0.09576 | 0.00327 | 0.01439 | 0.00023 | 93 | 3 | 92 | 1 |
| BSS8-12 | 2.28 | 0.04852 | 0.00084 | 0.09581 | 0.00165 | 0.01433 | 0.00022 | 93 | 2 | 92 | 1 |
| BSS8-13 | 1.76 | 0.04874 | 0.00094 | 0.09537 | 0.00181 | 0.01419 | 0.00020 | 92 | 2 | 91 | 1 |
| BSS8-14 | 1.30 | 0.04861 | 0.00185 | 0.09756 | 0.00360 | 0.01456 | 0.00025 | 95 | 3 | 93 | 2 |
| BSS8-15 | 1.53 | 0.04910 | 0.00118 | 0.09537 | 0.00220 | 0.01409 | 0.00020 | 92 | 2 | 90 | 1 |
| BSS8-16 | 1.29 | 0.04855 | 0.00075 | 0.09678 | 0.00148 | 0.01446 | 0.00019 | 94 | 1 | 93 | 1 |
| BSS8-17 | 1.38 | 0.04921 | 0.00308 | 0.09579 | 0.00575 | 0.01412 | 0.00033 | 93 | 5 | 90 | 2 |
| *Jingangshan pluton* | | | | | | | | | | | |
| 12JGS-5, coordinate: N24°02′39.4″, E117°30′01.7″ | | | | | | | | | | | |
| 12JGS5-01 | 1.65 | 0.04756 | 0.00078 | 0.08963 | 0.00164 | 0.01367 | 0.00020 | 87 | 2 | 88 | 1 |
| 12JGS5-02 | 1.96 | 0.05512 | 0.00124 | 0.10218 | 0.00240 | 0.01345 | 0.00021 | 99 | 2 | 86 | 1 |
| 12JGS5-03 | 1.37 | 0.04923 | 0.00112 | 0.09083 | 0.00207 | 0.01338 | 0.00018 | 88 | 2 | 86 | 1 |
| 12JGS5-04 | 1.65 | 0.05007 | 0.00094 | 0.09233 | 0.00181 | 0.01337 | 0.00018 | 90 | 2 | 86 | 1 |
| 12JGS5-05 | 1.63 | 0.04911 | 0.00096 | 0.08989 | 0.00186 | 0.01328 | 0.00020 | 87 | 2 | 85 | 1 |
| 12JGS5-06 | 1.54 | 0.04725 | 0.00215 | 0.08822 | 0.00395 | 0.01354 | 0.00026 | 86 | 4 | 87 | 2 |
| 12JGS5-07 | 1.75 | 0.05226 | 0.00199 | 0.09642 | 0.00363 | 0.01341 | 0.00026 | 93 | 3 | 86 | 2 |
| 12JGS5-08 | 1.97 | 0.05780 | 0.00733 | 0.10798 | 0.01316 | 0.01355 | 0.00052 | 104 | 12 | 87 | 3 |
| 12JGS5-09 | 1.36 | 0.04788 | 0.00086 | 0.08904 | 0.00158 | 0.01349 | 0.00020 | 87 | 1 | 86 | 1 |
| 12JGS5-10 | 1.31 | 0.04848 | 0.00066 | 0.08885 | 0.00122 | 0.01329 | 0.00019 | 86 | 1 | 85 | 1 |
| 12JGS5-11 | 1.92 | 0.05015 | 0.00066 | 0.09237 | 0.00121 | 0.01336 | 0.00018 | 90 | 1 | 86 | 1 |
| 12JGS5-12 | 2.60 | 0.05115 | 0.00708 | 0.09514 | 0.01285 | 0.01349 | 0.00046 | 92 | 12 | 86 | 3 |
| 12JGS5-13 | 2.57 | 0.04761 | 0.00427 | 0.08889 | 0.00782 | 0.01354 | 0.00031 | 86 | 7 | 87 | 2 |
| 12JGS5-14 | 1.23 | 0.04691 | 0.00167 | 0.08837 | 0.00302 | 0.01367 | 0.00024 | 86 | 3 | 88 | 2 |
| 12JGS5-15 | 1.25 | 0.04948 | 0.00204 | 0.09045 | 0.00352 | 0.01327 | 0.00027 | 88 | 3 | 85 | 2 |
| 12JGS5-16 | 2.18 | 0.04751 | 0.00216 | 0.08945 | 0.00398 | 0.01366 | 0.00023 | 87 | 4 | 87 | 1 |

| | | | | | | | | | | | |
|---|---|---|---|---|---|---|---|---|---|---|---|
| 12JGS5-17 | 2.72 | 0.04726 | 0.00482 | 0.08852 | 0.00887 | 0.01359 | 0.00031 | 86 | 8 | 87 | 2 |
| *Wushan pluton* | | | | | | | | | | | |
| 12WS-1, coordinate: N23°55'47.9", E117°11'11.6" | | | | | | | | | | | |
| 12WS1-01 | 1.19 | 0.04873 | 0.00117 | 0.09602 | 0.00224 | 0.01430 | 0.00022 | 93 | 2 | 92 | 1 |
| 12WS1-02 | 1.50 | 0.04819 | 0.00080 | 0.09606 | 0.00157 | 0.01447 | 0.00020 | 93 | 1 | 93 | 1 |
| 12WS1-03 | 1.61 | 0.04894 | 0.00097 | 0.09634 | 0.00188 | 0.01428 | 0.00020 | 93 | 2 | 91 | 1 |
| 12WS1-04 | 2.16 | 0.04958 | 0.00234 | 0.09574 | 0.00435 | 0.01402 | 0.00027 | 93 | 4 | 90 | 2 |
| 12WS1-05 | 3.55 | 0.04811 | 0.00120 | 0.09640 | 0.00234 | 0.01455 | 0.00022 | 93 | 2 | 93 | 1 |
| 12WS1-06 | 1.41 | 0.04831 | 0.00374 | 0.09460 | 0.00714 | 0.01422 | 0.00032 | 92 | 7 | 91 | 2 |
| 12WS1-07 | 3.05 | 0.04857 | 0.00244 | 0.09661 | 0.00475 | 0.01443 | 0.00025 | 94 | 4 | 92 | 2 |
| 12WS1-08 | 1.43 | 0.04566 | 0.00466 | 0.09320 | 0.00935 | 0.01483 | 0.00034 | 90 | 9 | 95 | 2 |
| 12WS1-09 | 1.22 | 0.05378 | 0.00228 | 0.10536 | 0.00433 | 0.01422 | 0.00024 | 102 | 4 | 91 | 2 |
| 12WS1-10 | 1.76 | 0.04928 | 0.00123 | 0.09685 | 0.00233 | 0.01426 | 0.00021 | 94 | 2 | 91 | 1 |
| 12WS1-11 | 0.74 | 0.05808 | 0.00333 | 0.11633 | 0.00644 | 0.01453 | 0.00029 | 112 | 6 | 93 | 2 |
| 12WS1-12 | 1.22 | 0.04798 | 0.00462 | 0.09519 | 0.00897 | 0.01439 | 0.00036 | 92 | 8 | 92 | 2 |
| 12WS1-13 | 1.95 | 0.04827 | 0.00268 | 0.09586 | 0.00522 | 0.01441 | 0.00024 | 93 | 5 | 92 | 2 |
| 12WS1-14 | 1.39 | 0.05512 | 0.00414 | 0.11231 | 0.00814 | 0.01478 | 0.00036 | 108 | 7 | 95 | 2 |
| 12WS1-15 | 1.48 | 0.04746 | 0.00094 | 0.09495 | 0.00184 | 0.01452 | 0.00020 | 92 | 2 | 93 | 1 |
| 12WS1-16 | 1.22 | 0.04868 | 0.00091 | 0.09800 | 0.00181 | 0.01460 | 0.00021 | 95 | 2 | 93 | 1 |
| 12WS1-17 | 1.89 | 0.05264 | 0.00210 | 0.10228 | 0.00399 | 0.01409 | 0.00023 | 99 | 4 | 90 | 1 |
| 12WS1-18 | 1.55 | 0.04874 | 0.00189 | 0.09462 | 0.00354 | 0.01408 | 0.00026 | 92 | 3 | 90 | 2 |
| 12WS-4, coordinate: N23°53'39.2", E117°09'41.9" | | | | | | | | | | | |
| 12WS4-01 | 1.63 | 0.05725 | 0.00641 | 0.11425 | 0.01248 | 0.01449 | 0.00043 | 110 | 11 | 93 | 3 |
| 12WS4-02 | 1.53 | 0.05649 | 0.00498 | 0.11299 | 0.00962 | 0.01451 | 0.00042 | 109 | 9 | 93 | 3 |
| 12WS4-03 | 1.35 | 0.04842 | 0.00083 | 0.09601 | 0.00180 | 0.01438 | 0.00021 | 93 | 2 | 92 | 1 |
| 12WS4-04 | 1.20 | 0.04793 | 0.00299 | 0.09570 | 0.00586 | 0.01450 | 0.00030 | 93 | 5 | 93 | 2 |
| 12WS4-05 | 0.97 | 0.05198 | 0.00148 | 0.10101 | 0.00286 | 0.01410 | 0.00022 | 98 | 3 | 90 | 1 |
| 12WS4-06 | 1.22 | 0.05426 | 0.00188 | 0.10529 | 0.00358 | 0.01409 | 0.00025 | 102 | 3 | 90 | 2 |
| 12WS4-07 | 1.08 | 0.04653 | 0.00086 | 0.09380 | 0.00182 | 0.01463 | 0.00020 | 91 | 2 | 94 | 1 |
| 12WS4-08 | 1.84 | 0.05176 | 0.00576 | 0.09974 | 0.01082 | 0.01399 | 0.00041 | 97 | 10 | 90 | 3 |
| 12WS4-09 | 1.70 | 0.04956 | 0.00382 | 0.09743 | 0.00735 | 0.01426 | 0.00031 | 94 | 7 | 91 | 2 |
| 12WS4-10 | 2.50 | 0.04896 | 0.00194 | 0.09618 | 0.00370 | 0.01426 | 0.00025 | 93 | 3 | 91 | 2 |
| 12WS4-11 | 2.14 | 0.04838 | 0.00126 | 0.09626 | 0.00245 | 0.01444 | 0.00021 | 93 | 2 | 92 | 1 |
| 12WS4-12 | 2.15 | 0.04837 | 0.00312 | 0.09520 | 0.00598 | 0.01429 | 0.00030 | 92 | 6 | 91 | 2 |
| 12WS4-13 | 1.84 | 0.04713 | 0.00363 | 0.09344 | 0.00706 | 0.01439 | 0.00029 | 91 | 7 | 92 | 2 |
| 12WS4-14 | 1.11 | 0.04877 | 0.00083 | 0.09481 | 0.00160 | 0.01410 | 0.00020 | 92 | 1 | 90 | 1 |
| 12WS4-15 | 1.64 | 0.04675 | 0.00152 | 0.09423 | 0.00300 | 0.01463 | 0.00023 | 91 | 3 | 94 | 1 |
| 12WS4-16 | 4.13 | 0.04787 | 0.00550 | 0.09529 | 0.01079 | 0.01444 | 0.00036 | 92 | 10 | 92 | 2 |
| 12WS4-17 | 2.30 | 0.04727 | 0.00080 | 0.09492 | 0.00159 | 0.01457 | 0.00021 | 92 | 1 | 93 | 1 |
| 12WS4-18 | 0.91 | 0.04748 | 0.00090 | 0.09484 | 0.00177 | 0.01449 | 0.00022 | 92 | 2 | 93 | 1 |
| 12WS4-19 | 2.31 | 0.04832 | 0.00580 | 0.09568 | 0.01123 | 0.01435 | 0.00042 | 93 | 10 | 92 | 3 |

Note: uncertainties of the measured isotope ratios are absolute.

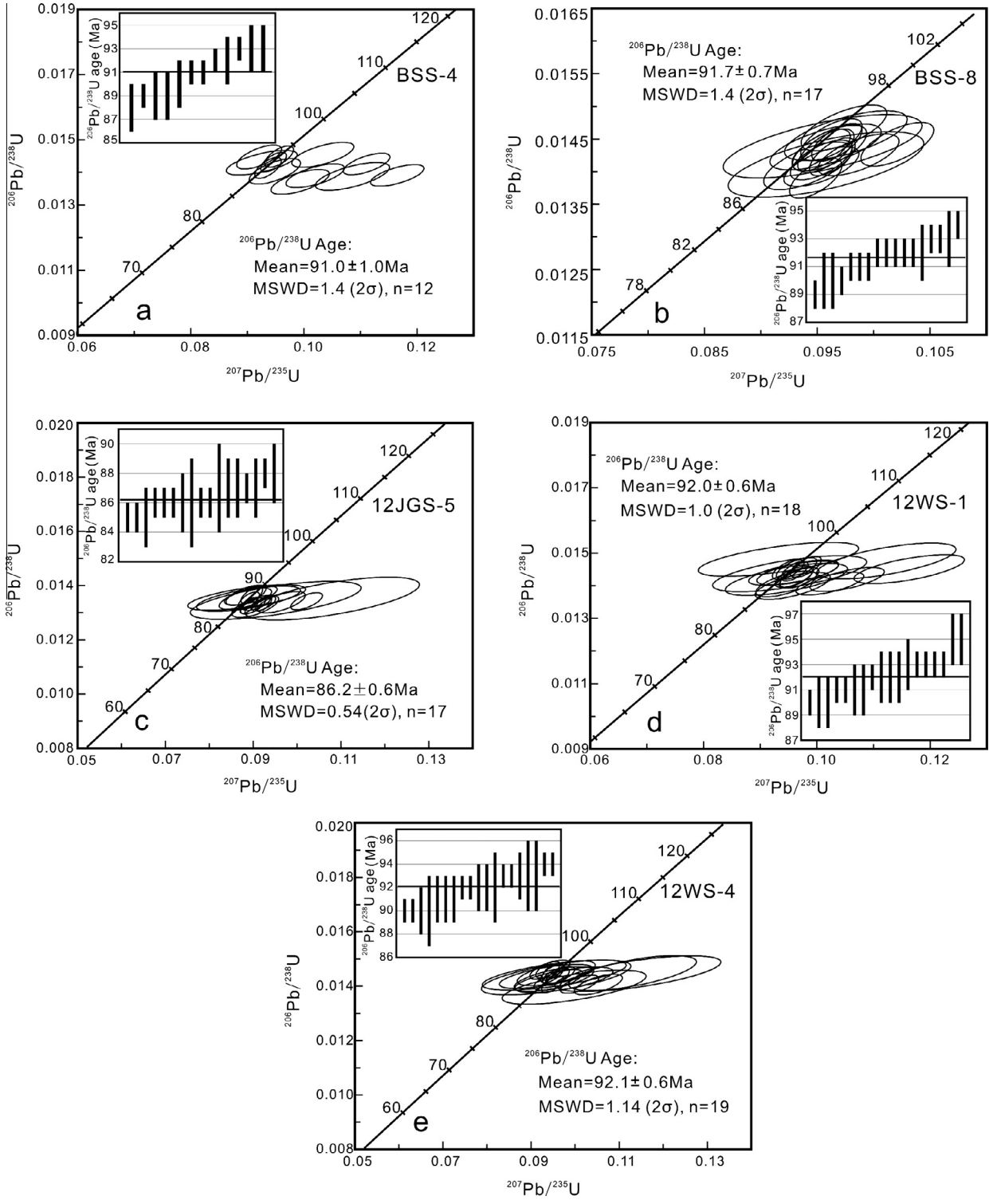


**Fig. 5.** Zircon U–Pb concordia diagrams of granites from Baishishan (BSS-4 and BSS-8), Jingangshan (12JGS-5) and Wushan (12WS-1 and 12WS-4) plutons.

(e.g., Ba = 29.08–538.53 ppm, Sr = 5.00–118.13 ppm, and Eu = 0.07–1.05 ppm), but the major element compositions show only slight variations; sample 12WS-3 from the marginal facies seems to be the least evolved of all the samples.

### 5.3. Whole-rock Nd isotopes

The whole-rock Nd isotopic compositions of representative granitic rocks from the Baishishan, Jingangshan, and Wushan plutons are listed in Table 3 and displayed in Fig. 8. All of the $\varepsilon_{Nd}(t)$ values and two-stage Nd model ages ($T_{DM2}$) were calculated using the crystallization ages obtained in this study. The samples from all three plutons show relatively high Sm and Nd contents, and $^{147}Sm/^{144}Nd$ ratios ranging from 0.102 to 0.150. They exhibit homogeneous Nd isotopic compositions, with initial $^{143}Nd/^{144}Nd$ ratios ranging from 0.512263 to 0.512359. The corresponding $\varepsilon_{Nd}(t)$ values and two-stage Nd model ages ($T_{DM2}$) are in the range of −3.3 to −5.0 and 1.16 to 1.30 Ga, respectively.

**Table 2**
Major (wt.%) and trace element (ppm) compositions of granites in the Baishishan, Jingangshan and Wushan plutons.

| Sample | Baishishan | | | | | | Jingangshan | | | | | | Wushan | | | | | | |
|---|---|---|---|---|---|---|---|---|---|---|---|---|---|---|---|---|---|---|---|
| | BSS-2 | BSS-4 | BSS-5 | BSS-6 | BSS-7 | BSS-8 | 12JGS-1 | 12JGS-3 | 12JGS-5 | 1[a] | 2[a] | 3[a] | 12WS-1 | 12WS-2 | 12WS-3 | 12WS-4 | 12WS-5 | WS-2[b] | WS-3[b] |
| $SiO_2$ | 77.05 | 76.69 | 75.81 | 78.15 | 78.09 | 76.97 | 76.1 | 76.98 | 75.18 | 75.21 | 76.87 | 76.78 | 75.34 | 75.91 | 75.46 | 76.31 | 75.93 | 78.04 | 78.79 |
| $TiO_2$ | 0.11 | 0.11 | 0.12 | 0.11 | 0.09 | 0.11 | 0.10 | 0.07 | 0.08 | 0.19 | 0.07 | 0.07 | 0.11 | 0.09 | 0.13 | 0.09 | 0.08 | 0.09 | 0.07 |
| $Al_2O_3$ | 11.66 | 12.06 | 12.53 | 12.09 | 11.96 | 11.83 | 12.31 | 11.89 | 12.73 | 12.92 | 12.55 | 12.36 | 12.68 | 12.37 | 12.68 | 12.30 | 12.28 | 12.06 | 11.56 |
| $Fe_2O_3^{tot}$ | 0.76 | 0.76 | 0.84 | 0.79 | 0.70 | 0.76 | 0.79 | 0.68 | 0.74 | 1.14 | 0.69 | 0.79 | 0.73 | 0.67 | 0.96 | 0.64 | 0.71 | 0.74 | 0.63 |
| MnO | 0.08 | 0.09 | 0.11 | 0.09 | 0.05 | 0.04 | 0.08 | 0.07 | 0.11 | 0.08 | 0.08 | 0.13 | 0.08 | 0.11 | 0.06 | 0.08 | 0.10 | 0.08 | 0.06 |
| MgO | 0.08 | 0.06 | 0.07 | 0.07 | 0.07 | 0.06 | 0.15 | 0.12 | 0.09 | 0.13 | 0.09 | 0.06 | 0.14 | 0.09 | 0.17 | 0.08 | 0.13 | 0.16 | 0.14 |
| CaO | 0.22 | 0.31 | 0.34 | 0.34 | 0.28 | 0.32 | 0.36 | 0.57 | 0.32 | 0.63 | 0.38 | 0.24 | 0.62 | 0.41 | 0.81 | 0.40 | 0.40 | 0.42 | 0.32 |
| $Na_2O$ | 4.06 | 4.08 | 4.29 | 4.09 | 4.10 | 4.03 | 4.36 | 3.95 | 4.58 | 3.88 | 4.04 | 3.94 | 4.08 | 4.38 | 4.05 | 4.09 | 4.38 | 4.04 | 3.84 |
| $K_2O$ | 4.11 | 4.37 | 4.52 | 4.29 | 4.39 | 4.40 | 4.28 | 4.16 | 4.34 | 4.67 | 4.27 | 4.29 | 4.27 | 4.22 | 4.27 | 4.30 | 4.13 | 3.98 | 3.88 |
| $P_2O_5$ | 0.04 | 0.02 | 0.02 | 0.02 | 0.02 | 0.02 | 0.01 | 0.01 | 0.01 | 0.02 | 0.01 | 0.01 | 0.02 | 0.01 | 0.03 | 0.02 | 0.02 | 0.03 | 0.03 |
| LOI | 0.56 | 0.34 | 0.42 | 0.40 | 0.52 | 0.44 | 0.52 | 0.98 | 0.38 | | | | 0.72 | 0.54 | 0.62 | 0.54 | 0.54 | | |
| Total | 98.7 | 98.9 | 99.1 | 100.4 | 100.3 | 99.0 | 99.1 | 99.5 | 98.6 | | | | 98.8 | 98.8 | 99.3 | 98.8 | 98.7 | | |
| $K_2O/Na_2O$ | 1.01 | 1.07 | 1.05 | 1.05 | 1.07 | 1.09 | 0.98 | 1.05 | 0.95 | 1.20 | 1.06 | 1.09 | 1.05 | 0.96 | 1.05 | 1.05 | 0.94 | 0.99 | 1.01 |
| ALK | 8.18 | 8.45 | 8.81 | 8.38 | 8.50 | 8.43 | 8.65 | 8.11 | 8.92 | 8.55 | 8.31 | 8.23 | 8.35 | 8.60 | 8.32 | 8.39 | 8.51 | 8.02 | 7.72 |
| A.R | 5.33 | 4.88 | 5.01 | 4.86 | 5.06 | 4.94 | 5.30 | 4.46 | 5.32 | 3.68 | 4.33 | 4.34 | 4.16 | 5.12 | 4.00 | 4.63 | 5.07 | 4.60 | 4.66 |
| A/NK | 1.05 | 1.05 | 1.05 | 1.06 | 1.04 | 1.04 | 1.04 | 1.08 | 1.04 | 1.13 | 1.11 | 1.11 | 1.12 | 1.05 | 1.12 | 1.08 | 1.05 | 1.10 | 1.10 |
| A/CNK | 1.01 | 1.00 | 1.00 | 1.01 | 0.99 | 0.99 | 0.99 | 0.99 | 0.99 | 1.03 | 1.05 | 1.07 | 1.02 | 0.99 | 0.99 | 1.01 | 0.99 | 1.03 | 1.04 |
| D.I | 97.7 | 97.3 | 97.1 | 97.1 | 97.7 | 97.5 | 97.1 | 96.2 | 97.4 | 94.8 | 96.5 | 96.9 | 95.4 | 97.1 | 94.4 | 96.8 | 96.9 | 96.3 | 96.9 |
| Sc | 2.21 | 2.63 | 2.69 | 1.54 | 1.48 | 2.48 | 2.11 | 2.33 | 2.34 | 4.60 | 2.60 | 2.86 | 3.49 | 1.28 | 3.10 | 2.95 | 3.93 | | |
| V | 0.83 | 0.58 | 0.58 | 1.19 | 0.56 | 0.71 | 1.03 | 0.80 | 0.87 | 3.95 | 1.50 | 1.50 | 4.65 | 2.30 | 8.91 | 2.32 | 2.27 | | |
| Cr | 2.00 | 1.28 | 1.86 | 0.75 | 0.76 | 1.41 | 2.63 | 2.56 | 3.65 | 9.68 | 9.77 | 10.44 | 0.80 | 1.42 | 1.26 | 1.92 | 1.45 | | |
| Co | 0.07 | 0.03 | 0.03 | 0.06 | 0.03 | 0.04 | 0.06 | 0.06 | 0.06 | | | | 0.36 | 0.15 | 0.72 | 0.18 | 0.16 | | |
| Ni | 0.72 | 0.57 | 0.74 | 0.29 | 0.17 | 0.39 | 1.04 | 1.09 | 1.87 | 4 | 4 | 4 | 0.27 | 0.64 | 0.77 | 1.15 | 0.66 | | |
| Cu | 1.15 | 0.73 | 0.85 | 0.69 | 0.63 | 0.74 | 0.80 | 0.85 | 0.82 | | | | 0.97 | 0.59 | 1.15 | 0.95 | 0.87 | | |
| Zn | 20.92 | 32.09 | 31.61 | 16.44 | 18.36 | 29.26 | 21.38 | 19.42 | 33.86 | | | | 28.56 | 17.66 | 36.06 | 28.81 | 15.63 | | |
| Ga | 16.76 | 19.22 | 20.70 | 16.70 | 16.74 | 18.15 | 20.06 | 21.09 | 22.81 | 17.43 | 19.09 | 20.09 | 21.70 | 19.44 | 21.10 | 22.06 | 22.58 | 17 | 17 |
| Rb | 205.14 | 237.67 | 239.24 | 240.28 | 253.26 | 241.83 | 277.39 | 333.38 | 310.00 | 169 | 200 | 222 | 334.87 | 376.92 | 221.76 | 291.98 | 381.63 | 224 | 229 |
| Sr | 6.86 | 4.66 | 6.35 | 4.76 | 5.02 | 4.91 | 4.66 | 12.77 | 3.57 | 29.30 | 7.03 | 5.72 | 94.62 | 11.53 | 118.13 | 28.40 | 13.06 | 5 | 5 |
| Y | 21.06 | 43.34 | 30.65 | 22.75 | 19.16 | 29.39 | 22.91 | 26.09 | 25.21 | 23.79 | 30.21 | 31.68 | 15.92 | 12.93 | 31.27 | 19.00 | 16.41 | 32 | 33 |
| Zr | 126.90 | 130.63 | 159.30 | 163.13 | 132.36 | 145.54 | 118.22 | 111.63 | 108.32 | 170 | 62 | 69 | 115.44 | 143.21 | 121.87 | 102.84 | 115.30 | 90 | 78 |
| Nb | 21.98 | 23.49 | 27.24 | 25.65 | 24.32 | 23.92 | 29.99 | 32.96 | 30.11 | 22 | 27 | 30 | 34.20 | 35.38 | 22.19 | 25.97 | 35.42 | 25 | 25 |
| Cs | 2.91 | 2.89 | 2.80 | 3.52 | 3.74 | 3.75 | 3.56 | 2.78 | 7.06 | | | | 4.99 | 3.21 | 3.78 | 2.62 | 3.38 | | |
| Ba | 18.96 | 14.81 | 14.78 | 16.92 | 14.67 | 17.20 | 19.93 | 19.78 | 20.41 | 205.30 | 17.20 | 17.89 | 476.57 | 29.08 | 538.53 | 118.22 | 44.16 | 74 | 74 |
| La | 19.36 | 26.92 | 22.62 | 23.40 | 18.04 | 26.13 | 30.30 | 19.71 | 22.90 | 58.87 | 38.71 | 30.47 | 26.69 | 29.26 | 30.23 | 24.55 | 24.08 | 25.34 | 21.78 |
| Ce | 33.92 | 50.39 | 49.29 | 44.50 | 35.76 | 50.04 | 55.19 | 39.30 | 45.15 | 112.80 | 61.40 | 60.04 | 48.42 | 51.47 | 52.48 | 46.48 | 39.54 | 45.30 | 35.88 |
| Pr | 4.92 | 6.13 | 6.02 | 5.26 | 4.22 | 6.03 | 5.85 | 4.05 | 4.78 | 12.48 | 7.37 | 6.21 | 4.60 | 3.66 | 5.77 | 4.10 | 3.29 | 4.91 | 3.93 |
| Nd | 16.37 | 21.84 | 20.24 | 17.98 | 13.85 | 18.72 | 16.64 | 12.27 | 13.69 | 40.94 | 22.05 | 18.60 | 14.11 | 8.86 | 18.47 | 11.95 | 8.13 | 16.18 | 12.71 |
| Sm | 3.98 | 5.43 | 5.02 | 3.95 | 3.05 | 4.22 | 3.13 | 2.59 | 2.84 | 7.28 | 4.86 | 4.05 | 2.46 | 1.29 | 3.80 | 2.02 | 1.11 | 3.43 | 2.65 |
| Eu | 0.18 | 0.21 | 0.17 | 0.14 | 0.14 | 0.18 | 0.16 | 0.11 | 0.15 | 1.05 | 0.44 | 0.37 | 0.30 | 0.07 | 0.55 | 0.15 | 0.09 | 0.19 | 0.14 |
| Gd | 3.55 | 5.84 | 4.79 | 3.77 | 2.84 | 4.15 | 2.82 | 2.53 | 2.76 | 5.18 | 4.42 | 3.32 | 2.09 | 1.11 | 3.69 | 1.90 | 1.11 | 3.68 | 3.07 |
| Tb | 0.56 | 0.87 | 0.69 | 0.55 | 0.42 | 0.60 | 0.43 | 0.38 | 0.43 | 0.99 | 0.92 | 0.83 | 0.29 | 0.17 | 0.52 | 0.29 | 0.17 | 0.66 | 0.55 |
| Dy | 4.15 | 6.98 | 5.13 | 3.94 | 3.10 | 4.64 | 3.39 | 3.39 | 3.47 | 5.58 | 5.72 | 4.78 | 2.21 | 1.34 | 3.92 | 2.53 | 1.47 | 4.34 | 3.67 |
| Ho | 0.90 | 1.53 | 1.17 | 0.88 | 0.71 | 0.96 | 0.77 | 0.81 | 0.86 | 1.03 | 1.23 | 1.05 | 0.50 | 0.37 | 0.98 | 0.57 | 0.42 | 1.03 | 0.86 |
| Er | 2.72 | 4.35 | 3.41 | 2.53 | 2.05 | 2.95 | 2.52 | 2.82 | 2.74 | 3.34 | 3.97 | 3.40 | 1.71 | 1.38 | 3.15 | 2.15 | 1.61 | 3.16 | 2.62 |
| Tm | 0.42 | 0.71 | 0.57 | 0.38 | 0.32 | 0.47 | 0.41 | 0.49 | 0.50 | 0.39 | 0.58 | 0.44 | 0.34 | 0.27 | 0.53 | 0.37 | 0.34 | 0.51 | 0.40 |
| Yb | 2.65 | 4.65 | 3.79 | 2.43 | 2.09 | 3.21 | 2.86 | 3.44 | 3.52 | 3.04 | 4.28 | 3.99 | 2.42 | 2.11 | 3.66 | 2.82 | 2.81 | 3.63 | 2.74 |
| Lu | 0.41 | 0.77 | 0.63 | 0.39 | 0.35 | 0.55 | 0.46 | 0.56 | 0.57 | 0.53 | 0.66 | 0.65 | 0.46 | 0.38 | 0.63 | 0.51 | 0.53 | 0.58 | 0.42 |
| Hf | 5.64 | 5.54 | 7.02 | 7.01 | 6.12 | 6.45 | 5.90 | 6.02 | 5.51 | | | | 5.54 | 8.17 | 4.88 | 5.30 | 6.39 | | |
| Ta | 1.99 | 2.25 | 2.35 | 2.13 | 2.09 | 2.15 | 2.65 | 2.44 | 2.28 | | | | 2.09 | 3.02 | 2.06 | 2.20 | 2.78 | | |
| Pb | 26.16 | 26.43 | 31.20 | 25.84 | 25.80 | 26.51 | 24.58 | 31.76 | 32.94 | | | | 30.6 | 32.88 | 25.33 | 30.85 | 30.64 | | |
| Th | 24.54 | 27.74 | 30.48 | 26.08 | 24.45 | 28.26 | 27.11 | 27.58 | 33.90 | | | | 26.64 | 37.15 | 22.69 | 25.55 | 31.30 | 26 | 25 |
| U | 5.76 | 7.08 | 8.59 | 8.24 | 5.28 | 7.66 | 7.81 | 6.43 | 10.16 | | | | 9.66 | 17.47 | 4.92 | 11.03 | 15.69 | 6 | 6 |

(*continued on next page*)

**Table 2** (*continued*)

| Sample | Baishishan | | | | | | Jingangshan | | | | | Wushan | | | | | | |
|---|---|---|---|---|---|---|---|---|---|---|---|---|---|---|---|---|---|---|
| | BSS-2 | BSS-4 | BSS-5 | BSS-6 | BSS-7 | BSS-8 | 12JGS-1 | 12JGS-3 | 12JGS-5 | 1[a] | 2[a] | 3[a] | 12WS-1 | 12WS-2 | 12WS-3 | 12WS-4 | 12WS-5 | WS-2[b] | WS-3[b] |
| ∑REE | 94.1 | 136.6 | 123.5 | 110.1 | 86.9 | 122.9 | 124.9 | 92.4 | 104.4 | 253.5 | 156.6 | 138.2 | 106.6 | 101.8 | 128.4 | 100.4 | 84.70 | 112.9 | 91.4 |
| LREE/HREE | 5.13 | 4.31 | 5.12 | 6.40 | 6.32 | 6.01 | 8.13 | 5.41 | 6.02 | 11.62 | 6.19 | 6.49 | 9.64 | 13.26 | 6.52 | 8.00 | 9.01 | 5.42 | 5.38 |
| $(La/Yb)_N$ | 4.92 | 3.90 | 4.03 | 6.50 | 5.81 | 5.49 | 7.14 | 3.87 | 4.39 | 13.06 | 6.10 | 5.15 | 7.45 | 9.34 | 5.57 | 5.87 | 5.78 | 5.01 | 5.70 |
| $(La/Sm)_N$ | 3.06 | 3.12 | 2.83 | 3.73 | 3.72 | 3.90 | 6.09 | 4.78 | 5.07 | 5.09 | 5.01 | 4.73 | 6.83 | 14.32 | 5.00 | 7.63 | 13.68 | 4.65 | 5.17 |
| $(Gd/Yb)_N$ | 1.08 | 1.01 | 1.02 | 1.25 | 1.10 | 1.04 | 0.80 | 0.59 | 0.63 | 1.38 | 0.83 | 0.67 | 0.70 | 0.43 | 0.81 | 0.54 | 0.32 | 0.82 | 0.90 |
| Eu/Eu* | 0.14 | 0.11 | 0.11 | 0.11 | 0.14 | 0.13 | 0.16 | 0.13 | 0.16 | 0.52 | 0.29 | 0.31 | 0.41 | 0.17 | 0.45 | 0.23 | 0.24 | 0.16 | 0.15 |
| Rb/Sr | 29.91 | 51.05 | 37.65 | 50.45 | 50.47 | 49.25 | 59.47 | 26.11 | 86.75 | 5.77 | 28.45 | 38.81 | 3.54 | 32.68 | 1.88 | 10.28 | 29.23 | 44.80 | 45.80 |
| Rb/Ba | 10.82 | 16.04 | 16.18 | 14.20 | 17.27 | 14.06 | 13.92 | 16.85 | 15.19 | 0.82 | 11.63 | 12.41 | 0.70 | 12.96 | 0.41 | 2.47 | 8.64 | 3.03 | 3.09 |
| 10000 × Ga/Al | 2.72 | 3.01 | 3.12 | 2.61 | 2.64 | 2.90 | 3.08 | 3.35 | 3.38 | 2.55 | 2.87 | 3.07 | 3.23 | 2.97 | 3.14 | 3.39 | 3.47 | 2.66 | 2.78 |
| Zr + Nb + Ce + Y | 203.9 | 247.8 | 266.5 | 256 | 211.6 | 248.9 | 226.3 | 210.0 | 208.8 | 328.6 | 180.6 | 190.7 | 214.0 | 243.0 | 227.8 | 194.3 | 206.7 | 192.3 | 171.9 |

Note: LOI: loss on ignition; D.I: differentiation index; A/CNK = $Al_2O_3/(CaO + Na_2O + K_2O)$ (mol%); A/NK = $Al_2O_3/(Na_2O + K_2O)$ (mol%); alkalinity ratio (A.R.) = $(Al_2O_3 + CaO + ALK)/(Al_2O_3 + CaO-ALK)$ (wt.%), notes that ALK value is twice wt.% content of the $Na_2O$, when $SiO_2 > 50$ wt.%, $2.5 > K_2O/Na_2O > 1$.

[a] Data from Hong et al. (1987).

[b] Data from Qiu et al. (2004).

### 5.4. Zircon Hf isotopes

In situ Lu–Hf isotopic analyses of zircons were performed on the same five samples selected for zircon U–Pb dating. The analytical results are given in Table 4 and graphically presented in Figs. 9 and 10.

The Hf isotopic analyses for zircon grains from the two Baishishan pluton samples (BSS-4 and BSS-8) show homogeneous Hf isotopic compositions, with initial $^{176}Hf/^{177}Hf$ ratios of 0.282596–0.282723 and 0.282639–0.282718, corresponding to $\varepsilon_{Hf}(t)$ values of −4.2 to + 0.3 (average, −1.7) and −2.7 to +0.1 (average, −0.1), respectively (Fig. 9a and b), and $T_{DM2}$ model ages of 1.14–1.42 Ga and 1.15–1.33 Ga, respectively.

Twenty zircon grains from Jingangshan (12JGS-5) gave initial $^{176}Hf/^{177}Hf$ ratios of 0.282605–0.282730 and $\varepsilon_{Hf}(t)$ values of −4.0 to +0.4 (average, −1.0) (Fig. 9c). The corresponding two-stage Hf model ages ($T_{DM2}$) vary from 1.13 Ga to 1.41 Ga.

The zircons from the two samples of the Wushan pluton (12WS-1 and 12WS-4) show almost identical Hf isotopic compositions, with initial $^{176}Hf/^{177}Hf$ ratios of 0.282622–0.282718 and 0.282631–0.282747; calculated $\varepsilon_{Hf}(t)$ values are in the range of −3.3 to +0.1 and −3.0 to +1.1, respectively (Fig. 9d and e), corresponding to Mesoproterozoic $T_{DM2}$ model ages of 1.15–1.37 Ga and 1.08–1.35 Ga, respectively.

## 6. Discussion

### 6.1. Petrogenetic type: S-type, I-type or A-type?

Since the term "A-type granite" was first proposed by Loiselle and Wones (1979) to distinguish a special group of granites from other granites, various chemical parameters have been proposed as indicators of A-type granites, such as their high $FeO^{tot}/MgO$, $K_2O/Na_2O$, and Ga/Al ratios, high $Na_2O + K_2O$, Y, Nb, Ce, REE, and Ga concentrations, low Cr, V, Ni, Ba, Sr, and Eu contents, and flat HREE distribution patterns. Among them, high Ga/Al ratios and enrichment in HFSEs (e.g., Nb and Ta) are generally considered to be the most diagnostic signatures of A-type granitoids (Bonin, 2007; Collins et al., 1982; Eby, 1990, 1992; King et al., 1997; Whalen et al., 1987). However, distinguishing the highly fractionated A-type granites from other types of granites is not always straightforward, as their original characteristics are obscured during magma evolution. In the case of highly evolved A-type granites, their geochemical compositions and mineralogical assemblages may be similar to those of felsic, fractionated I-type, and fractionated S-type granites. Therefore, it is necessary to comprehensively integrate petrological, mineralogical, and geochemical criteria to identify the genetic type of A-type granites (Kemp et al., 2005; King et al., 1997; Whalen et al., 1987; Wu et al., 2002).

Generally, A- and I-type granites have lower $P_2O_5$ contents, lower A/CNK ratios (<1.1), higher $Na_2O$ contents, and are more depleted in Ba, Sr, and Eu relative to S-type granites (Chappell, 1999; Whalen et al., 1987, 1996; Wolf and London, 1994). The aforementioned geochemical data show that the three granitic plutons in this study all have low $P_2O_5$ contents (<0.04%) and metaluminous to weakly peraluminous signatures, with A/CNK ratios of 0.99–1.07; these characteristics are different from those of strongly peraluminous S-type granites.

With respect to the trace element signatures, the granites of the three plutons show some geochemical affinities with I-type granites, such as relatively low concentrations of Zr + Nb + Ce + Y (<350 ppm), Zr, Zn, and REEs (Table 2), which are traditionally thought to be the main characteristics distinguishing A-type granites from highly evolved I-type granites. Numerous studies have demonstrated that Zr, Y, and REEs (except for Eu) are hosted

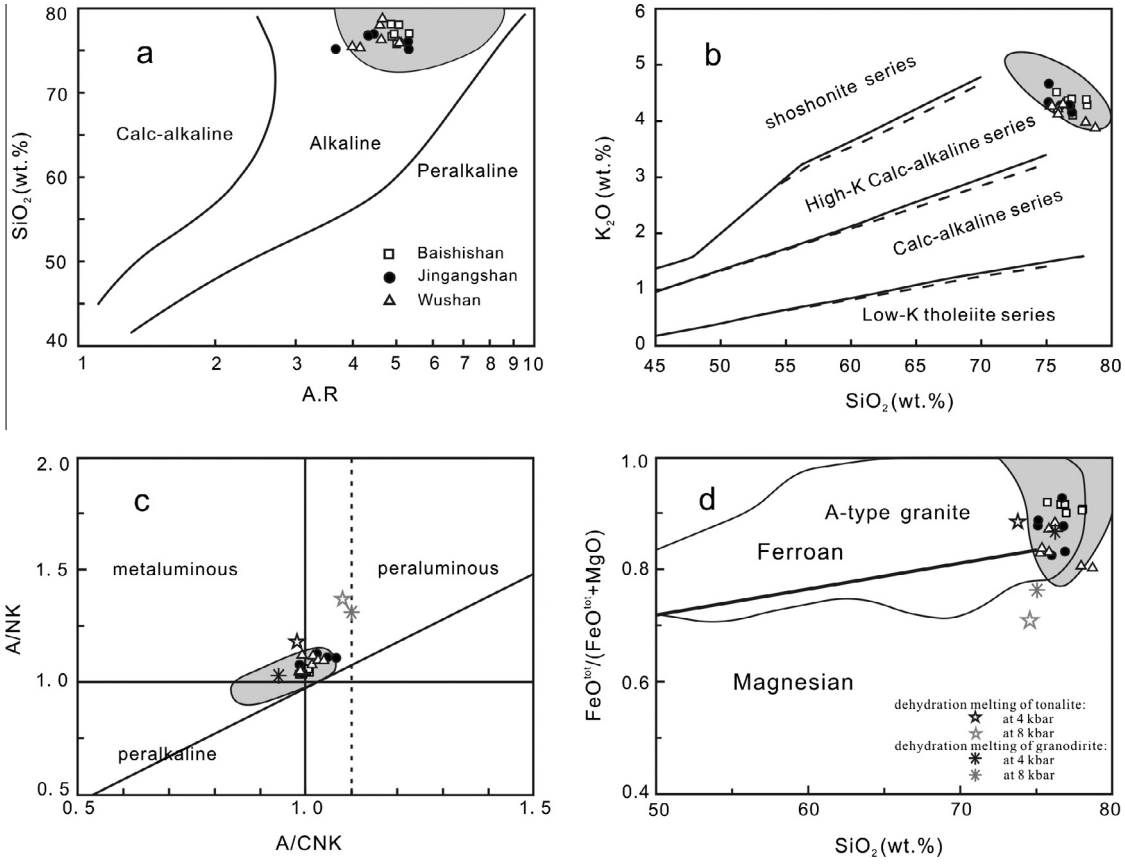


**Fig. 6.** (a) A.R *vs.* $SiO_2$ diagram (after Wright, 1969); (b) $SiO_2$ *vs.* $K_2O$ diagram (solid lines after Peccerillo and Taylor, 1976; dashed lines from Middlemost, 1985); (c) A/CNK *vs.* A/NK diagram (after Manilar and Piccoli, 1989); (d) $SiO_2$ *vs.* $FeO^{tot}/(FeO^{tot} + MgO)$ diagram (after Frost et al., 2001). Compositions of melts from melting experiments are after Patiño Douce (1997). A-type granites (shaded area) emplaced in the coastal area of Fujian and Zhejiang Provinces are also shown in these plots, and the data sources are from Dong and Peng (1994), Li et al. (2011), Qiu et al. (1999a, 2004) and Xiao et al. (2007).

mainly in zircon, apatite, monazite, titanite, allanite, ilmenite, and amphibole, based on the different partition coefficients of these elements (Arth, 1976; Rollinson, 1993). The fractional crystallization of zircon and amphibole has a significant effect on the concentrations of Zr, thus leading Zr contents to decrease with increasing fractionation in both A- and I-type granites (King et al., 1997). For example, it has been reported that concentrations of Zr are ~100 ppm in some samples of aluminous A-type granites from the Lachlan Fold Belt of Australia (King et al., 1997), and as low as 55 ppm in samples of A-type granites from northeastern China (Wu et al., 2002). The low Zr contents in the highly evolved granites in the present study may have resulted from the separation of Zr-rich minerals, such as zircon, which is a ubiquitous accessory mineral in these rocks. In addition, as the Zr contents have a direct and significant impact on (Zr + Nb + Ce + Y) values, the use of chemical discrimination diagrams based on Zr contents should be treated with caution, especially in distinguishing strongly fractionated A-type granites from similarly evolved I-type granites.

However, granites of the three plutons in this study have relatively high $K_2O + Na_2O$ contents (7.72–8.92 wt.%) and high $(K_2O + Na_2O)/CaO$ (10.27–36.70), Nb/Ta (10.45–16.37), Zr/Hf (17.54–24.97), and Ga/Al ratios, and thus resemble typical differentiated A-type granites (Eby, 1992; King et al., 1997; Martin et al., 1994; Whalen et al., 1987; Wong et al., 2009). As compared with the highly evolved felsic granites exposed in the coastal area of SE China (Fig. 7), the trace element signatures of granites from the three studied plutons are much closer to those observed in Xincun A-type granites, e.g., their high Nb and Ta concentrations (Chen et al., 2013; Qiu et al., 2004). However, the trace element signatures of the studied granites are quite different from those of I-type granites (Qiu et al., 2008, 2012; Zhao et al., 2012). King et al. (1997) found that concentrations of Ba, Sr, P, Ti, and Eu are commonly more strongly depleted in A-type granites than in I-type granites; the strong depletion of these elements is regarded as another typical signature of the A-type granites cropping out in the coastal area of SE China (Chen et al., 2000), which is in accordance with the patterns shown in the spidergrams for these three plutons (Fig. 7).

In the discrimination diagrams of $(K_2O + Na_2O)/CaO$, $K_2O/MgO$, and Nb *vs.* Ga/Al, and Ga/Al *vs.* $Eu/Eu^*$ (Fig. 11), all three of the studied plutons fall in the region of A-type granites. The following features are of particular interest. Nb contents are generally unaffected by fractional crystallization in A-type magmas (King et al., 1997) and are traditionally considered to be relatively insensitive to low–moderate degrees of alteration (Whalen et al., 1987). Thus, the high Nb contents in this study are another particularly diagnostic feature of A-type granites. Moreover, all zircon grains with signatures of magmatic origins have no inherited cores. Micrographic intergrowths of quartz and alkali feldspars are common in the studied granites. These features clearly indicate a high initial magmatic temperature for these granites, belonging to another typical characteristic of A-type granites (King et al., 1997, 2001). In summary, both petrographic and geochemical features argue strongly that the miarolitic alkali feldspar granites from the Baishishan, Jingangshan, and Wushan plutons are evolved A-type granites rather than highly fractionated I- or S-type granites. In combination with

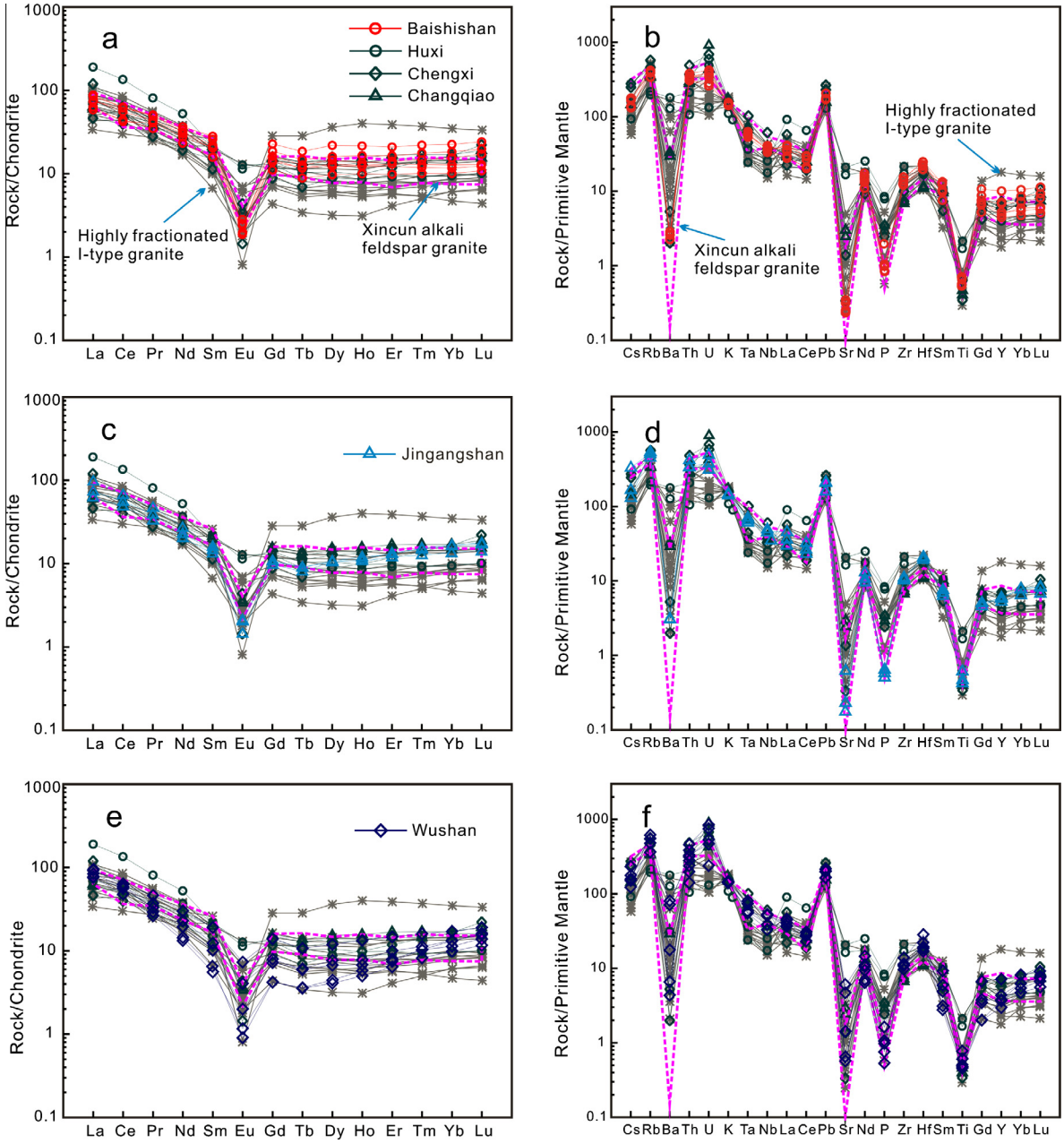


**Fig. 7.** Chondrite-normalized REE patterns (a, c and e) and primitive mantle-normalized spidergrams for the Baishishan, Jingangshan and Wushan granites (b, d and f). The normalization values for chondrite and primitive mantle are from Boynton (1984) and McDonough and Sun (1995), respectively. Data sources: Changqiao, Chengxi and Huxi intrusions of the Zhangpu composite granite pluton from Qiu et al. (2012); Xincun alkali feldspar granites from Chen et al. (2013); Highly fractionated granite from Qiu et al. (2008) and Zhao et al. (2012).

their metaluminous to weakly peraluminous signatures, and the occurrence of aluminum-rich minerals (e.g., spessartine and muscovite; Qiu et al., 2004), the granites in the three plutons can be further classified as aluminous A-type granites, according to the classification scheme of King et al. (1997).

### 6.2. Potential magma sources

Although a broad consensus has been reached concerning the tectonic setting and geochemical features of A-type granites, the origins of such granites are still quite controversial. Several petrogenetic models have been proposed to explain the origin of A-type granites, as described in the Introduction section. Among these models, the debates have focused on both the nature of the source rocks and the role of mantle-derived magma in the generation of A-type granites (Chen et al., 2013; Whalen et al., 1996; Wu et al., 2002). Likewise, for the Baishishan, Jingangshan, and Wushan granites, the two issues are also important in deciphering their petrogenesis.

As mentioned above, there are many similarities in petrography and in major and trace element compositions among the three studied granites, implying their derivation from a similar or common source, and from multiple occurrences of the same magmatic process. Moreover, they show similar whole-rock Nd isotopic composition and mutually overlapping zircon Hf isotopic compositions (Figs. 8 and 10), and the calculated two-stage Hf isotopic model

**Table 3**
Nd isotopic compositions of the Baishishan, Jingangshan and Wushan plutons.

| Sample | Age (Ma) | Sm (ppm) | Nd (ppm) | Sm/Nd | $^{147}Sm/^{144}Nd$ | $^{143}Nd/^{144}Nd$ | $2\sigma$ | $(^{143}Nd/^{144}Nd)_i$ | $\varepsilon_{Nd}(t)$ | $T_{DM2}$ (Ga) |
|---|---|---|---|---|---|---|---|---|---|---|
| BSS-2 | 91 | 3.98 | 16.37 | 0.24 | 0.147 | 0.512438 | 10 | 0.512351 | −3.3 | 1.16 |
| BSS-4 | 91 | 5.43 | 21.84 | 0.25 | 0.150 | 0.512419 | 6 | 0.512330 | −3.7 | 1.20 |
| BSS-6 | 91 | 3.95 | 17.98 | 0.22 | 0.133 | 0.512414 | 6 | 0.512335 | −3.6 | 1.19 |
| BSS-8 | 91 | 4.22 | 18.72 | 0.23 | 0.136 | 0.512414 | 5 | 0.512333 | −3.7 | 1.19 |
| 12JGS-3 | 86 | 2.59 | 12.27 | 0.21 | 0.128 | 0.512431 | 6 | 0.512359 | −3.3 | 1.16 |
| 12JGS-5 | 86 | 2.84 | 13.69 | 0.21 | 0.125 | 0.512429 | 6 | 0.512359 | −3.3 | 1.16 |
| JG-5[a] | 86 | 3.09 | 14.83 | 0.21 | 0.126 | 0.512372 | 8 | 0.512301 | −4.4 | 1.25 |
| JG-9[a] | 86 | 3.45 | 16.57 | 0.21 | 0.126 | 0.512376 | 8 | 0.512305 | −4.3 | 1.24 |
| 12WS-1 | 92 | 2.46 | 14.11 | 0.17 | 0.105 | 0.512416 | 7 | 0.512353 | −3.3 | 1.16 |
| 12WS-3 | 92 | 3.80 | 18.47 | 0.21 | 0.124 | 0.512382 | 10 | 0.512307 | −4.2 | 1.23 |
| 12WS-4 | 92 | 2.02 | 11.95 | 0.17 | 0.102 | 0.512376 | 11 | 0.512314 | −4.0 | 1.22 |
| WS-3[a] | 92 | 2.73 | 12.59 | 0.22 | 0.131 | 0.512342 | 7 | 0.512263 | −5.0 | 1.30 |

Note: $\varepsilon_{Nd}(t) = \{[(^{143}Nd/^{144}Nd)_s - (^{147}Sm/^{144}Nd)_s \times (e^{\lambda t} - 1)]/[(^{143}Nd/^{144}Nd)_{CHUR,0} - (^{147}Sm/^{144}Nd)_{CHUR,0} \times (e^{\lambda t} - 1)] - 1\} \times 10{,}000$.
$T_{DM2} = 1/\lambda \times \ln\{1 + [(^{143}Nd/^{144}Nd)_s - (^{143}Nd/^{144}Nd)_{DM} - ((^{147}Sm/^{144}Nd)_s - (^{147}Sm/^{144}Nd)_{cc}) \times (e^{\lambda t} - 1)]/[(^{147}Sm/^{144}Nd)_{cc} - (^{147}Sm/^{144}Nd)_{DM}]\}$.
Chondrite uniform reservoir (CHUR) values: $(^{147}Sm/^{144}Nd)_{CHUR,0} = 0.1967$, $(^{143}Nd/^{144}Nd)_{CHUR,0} = 0.512638$ (Miller and O'Nions, 1985); depleted mantle values: $(^{147}Sm/^{144}Nd)_{DM} = 0.513151$, $(^{143}Nd/^{144}Nd)_{DM} = 0.513151$ (Miller and O'Nions, 1985); $(^{147}Sm/^{144}Nd)_{cc} = 0.118$ (Jahn and Condie, 1995); $\lambda = 6.54 \times 10^{-12}$ year$^{-1}$ (Lugmair and Harti, 1978).
[a] Data came from Qiu et al. (2004).

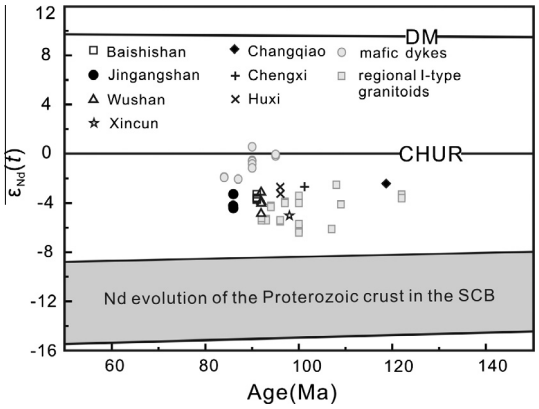


**Fig. 8.** Age *vs.* $\varepsilon_{Nd}(t)$ values diagram for samples from the Baishishan, Jingangshan and Wushan granites. DM–depleted mantle; CHUR – chondritic uniform reservoir. The Preoterozoic crustal evolutionary area of South China Block is after Shen et al. (1993). Data sources: Changqiao, Chengxi and Huxi intrusion from the Zhangpu composite granite pluton (Qiu et al., 2012); Xincun alkli feldspar granites (Chen et al., 2013); part of the data of the Baishishan, Jingangshan and Wushan granites after Qiu et al. (2004); mafic dykes from Qin et al. (2010), Dong et al. (2006, 2011), Zhang et al. (2007); regional I-type granitoids from Chen et al. (2013), Martin et al. (1994), Qiu et al. (1999a, 2008), Zhou and Chen (2001).

ages are broadly consistent with corresponding whole-rock Nd isotopic model ages, further suggesting their origination from a common source.

In the coastal area of Zhejiang and Fujian Provinces, SE China, A-type granites are always spatially associated with earlier emplaced I-type granitoids, and exhibit more fractionated geochemical characteristics than do the latter, usually with $SiO_2$ contents of more than 74 wt.% (e.g., the Kuiqi, Qingtian, Taohuadao, and Xincun plutons). There is now a general consensus among geologists that a significant amount of mantle-derived magma was involved in the generation of these I-type granites, resulting in their high radiogenic Nd–Hf isotopic compositions and the occurrence of mafic microgranular enclaves (Griffin et al., 2002; Qiu et al., 2008, 2012; Xu et al., 1999; Zhou et al., 2006). Such a magma-mixing model has also been used to explain the origins of A-type granites, based on the close field relationships and similar isotopic characteristics of the A- and I-type granites in the coastal area of SE China (Li et al., 2011; Xiao et al., 2007). However, it is difficult to reconcile the absence of mingling structures and mafic microgranular enclaves in the A-type plutons exposed in the coastal area of SE China, as these features are considered to be good indicators of the mixed origin of A-type granites (Karsli et al., 2012; Yang et al., 2006). Moreover, a distinctive isotopic feature commonly observed in the Baishishan, Jingangshan, and Wushan granites is their homogeneous zircon Hf isotopic compositions, with $\varepsilon_{Hf}(t)$ values ranging mostly from −3.0 to +1.1, which differs from the $\varepsilon_{Hf}(t)$ values of the coexisting Zhangpu composite granite pluton and the coeval highly fractionated I-type plutons in coastal areas of Fujian Province. It is reported that in these I-type granitoids, zircon $\varepsilon_{Hf}(t)$ values vary over a range of 6 units, and even up to 14.8 units, and show bimodal or multi-peak distribution patterns (Figs. 9 and 10; Qiu et al., 2008, 2012). It should be especially noted that Hf isotopes in zircon can record the details of isotopic signatures inherited from primary magmas more faithfully than can whole-rock Sm–Nd and Rb–Sr isotope systems, meaning that Hf isotope data are the best indicator of the nature of magma sources and the role of magma mixing processes in the generation of granitoids (Belousova et al., 2006; Kemp et al., 2005; Shaw et al., 2011), as the closure temperature of Hf isotopes is higher than those of the Sm–Nd and Rb–Sr systems. Thus, the homogeneous Hf isotopic compositions, comprising narrow and unimodal distribution patterns of $\varepsilon_{Hf}(t)$ values (Fig. 9), further indicate that magma mixing may not be the major process for generation of the studied A-type granites.

The three studied A-type granite plutons, with a total outcrop area of over 490 km$^2$, are marked by weakly negative Nb–Ta anomalies and significant positive Pb anomalies in the spidergrams (Fig. 7), extremely high $SiO_2$ and low MgO, $FeO^{tot}$, and MnO concentrations, negative $\varepsilon_{Nd}(t)$ values, and low $\varepsilon_{Hf}(t)$ values, indicating that they were likely formed by partial melting of crustal materials. Moreover, the Ce/Pb and Nb/Ta ratios of these A-type granites are in the range of 1.3–2.3 and 10.4–16.4, respectively (averages of 1.6 and 12.1, respectively), which are lower than those of primitive mantle (Ce/Pb ≈ 9 and Nb/Ta ≈ 17.5) and close to those for continental crust (Ce/Pb ≈ 4 and Nb/Ta ≈ 11–12) (Green, 1995; Hofmann et al., 1986), suggesting their derivation from a crustal source. Based on zircon oxygen isotopic data, Wei et al. (2008) also indicated that A-type granites from eastern China were dominantly derived from crustal igneous rocks, as their zircon $\delta^{18}O$ values sharply conflict with a mantle origin. Accordingly, we conclude that the studied A-type granites were derived from the partial melting of pre-existing crustal rocks.

Detailed U–Pb dating and Lu–Hf analyses of detrital zircons from SE China have revealed that there were two important episodes of juvenile crustal formation (1.85–1.87 Ga, and

**Table 4**
Zircon in-situ Hf isotopic compositions for the Baishishan, Jingangshan and Wushan plutons.

| Spot | $^{176}Lu/^{177}Hf$ | $^{176}Hf/^{177}Hf$ | $2\sigma$ | $^{176}Yb/^{177}Hf$ | $(^{176}Hf/^{177}Hf)_i$ | $\varepsilon_{Hf}(t)$ | $2\sigma$ | $T_{DM1}$ (Ga) | $T_{DM2}$ (Ga) |
|---|---|---|---|---|---|---|---|---|---|
| *Baishishan: BSS-4* | | | | | | | | | |
| BSS-4-01 | 0.002075 | 0.282686 | 0.000017 | 0.056150 | 0.282682 | −1.2 | 0.6 | 0.83 | 1.23 |
| BSS-4-02 | 0.002944 | 0.282679 | 0.000012 | 0.074427 | 0.282674 | −1.5 | 0.4 | 0.86 | 1.25 |
| BSS-4-03 | 0.003832 | 0.282694 | 0.000016 | 0.100974 | 0.282688 | −1.0 | 0.6 | 0.85 | 1.22 |
| BSS-4-04 | 0.002908 | 0.282709 | 0.000014 | 0.080531 | 0.282704 | −0.4 | 0.5 | 0.81 | 1.18 |
| BSS-4-05 | 0.002506 | 0.282601 | 0.000020 | 0.062554 | 0.282596 | −4.2 | 0.7 | 0.96 | 1.42 |
| BSS-4-06 | 0.002807 | 0.282692 | 0.000014 | 0.074836 | 0.282688 | −1.0 | 0.5 | 0.83 | 1.22 |
| BSS-4-07 | 0.003103 | 0.28266 | 0.000017 | 0.083547 | 0.282655 | −2.1 | 0.6 | 0.89 | 1.29 |
| BSS-4-08 | 0.001707 | 0.282674 | 0.000018 | 0.045132 | 0.282671 | −1.6 | 0.7 | 0.83 | 1.26 |
| BSS-4-09 | 0.001496 | 0.282612 | 0.000016 | 0.039443 | 0.282610 | −3.8 | 0.6 | 0.92 | 1.40 |
| BSS-4-10 | 0.003133 | 0.282663 | 0.000016 | 0.085065 | 0.282658 | −2.0 | 0.6 | 0.88 | 1.29 |
| BSS-4-11 | 0.002324 | 0.282683 | 0.000012 | 0.061324 | 0.282679 | −1.3 | 0.4 | 0.84 | 1.24 |
| BSS-4-12 | 0.001790 | 0.282677 | 0.000014 | 0.048338 | 0.282674 | −1.5 | 0.5 | 0.83 | 1.25 |
| BSS-4-13 | 0.002837 | 0.282683 | 0.000012 | 0.074036 | 0.282678 | −1.3 | 0.4 | 0.85 | 1.24 |
| BSS-4-14 | 0.003119 | 0.282638 | 0.000024 | 0.084096 | 0.282632 | −2.9 | 0.8 | 0.92 | 1.34 |
| BSS-4-15 | 0.002206 | 0.282727 | 0.000014 | 0.059206 | 0.282723 | 0.3 | 0.5 | 0.77 | 1.14 |
| BSS-4-16 | 0.002895 | 0.282695 | 0.000014 | 0.072566 | 0.282691 | −0.9 | 0.5 | 0.83 | 1.21 |
| BSS-4-17 | 0.002125 | 0.282681 | 0.000012 | 0.055822 | 0.282677 | −1.4 | 0.4 | 0.83 | 1.24 |
| BSS-4-18 | 0.003681 | 0.282652 | 0.000022 | 0.088568 | 0.282646 | −2.5 | 0.8 | 0.91 | 1.31 |
| BSS-4-19 | 0.002016 | 0.282669 | 0.000015 | 0.056388 | 0.282666 | −1.8 | 0.5 | 0.85 | 1.27 |
| *Baishishan: BSS-8* | | | | | | | | | |
| BSS-8-01 | 0.002420 | 0.282689 | 0.000017 | 0.059448 | 0.282684 | −1.1 | 0.6 | 0.83 | 1.23 |
| BSS-8-02 | 0.002521 | 0.282713 | 0.000013 | 0.062559 | 0.282708 | −0.3 | 0.4 | 0.80 | 1.17 |
| BSS-8-03 | 0.001983 | 0.282720 | 0.000013 | 0.055389 | 0.282717 | 0.1 | 0.4 | 0.77 | 1.15 |
| BSS-8-04 | 0.002972 | 0.282647 | 0.000019 | 0.073799 | 0.282642 | −2.6 | 0.7 | 0.90 | 1.32 |
| BSS-8-05 | 0.003465 | 0.282715 | 0.000018 | 0.091944 | 0.282709 | −0.2 | 0.6 | 0.81 | 1.17 |
| BSS-8-06 | 0.003137 | 0.282688 | 0.000023 | 0.093757 | 0.282682 | −1.2 | 0.8 | 0.85 | 1.23 |
| BSS-8-07 | 0.002258 | 0.282642 | 0.000013 | 0.059704 | 0.282639 | −2.7 | 0.5 | 0.89 | 1.33 |
| BSS-8-08 | 0.001569 | 0.282666 | 0.000018 | 0.040897 | 0.282663 | −1.9 | 0.6 | 0.84 | 1.27 |
| BSS-8-09 | 0.001587 | 0.282711 | 0.000016 | 0.043998 | 0.282708 | −0.3 | 0.6 | 0.78 | 1.17 |
| BSS-8-10 | 0.003254 | 0.282708 | 0.000014 | 0.086632 | 0.282703 | −0.5 | 0.5 | 0.82 | 1.18 |
| BSS-8-11 | 0.001855 | 0.282703 | 0.000016 | 0.051713 | 0.282700 | −0.6 | 0.6 | 0.80 | 1.19 |
| BSS-8-12 | 0.002031 | 0.282712 | 0.000013 | 0.055344 | 0.282709 | −0.3 | 0.5 | 0.79 | 1.17 |
| BSS-8-13 | 0.003130 | 0.282723 | 0.000018 | 0.095129 | 0.282718 | 0.1 | 0.6 | 0.79 | 1.15 |
| BSS-8-14 | 0.001453 | 0.282701 | 0.000019 | 0.042572 | 0.282699 | −0.6 | 0.7 | 0.79 | 1.19 |
| BSS-8-15 | 0.003462 | 0.282650 | 0.000020 | 0.084324 | 0.282644 | −2.5 | 0.7 | 0.91 | 1.32 |
| BSS-8-16 | 0.002847 | 0.282720 | 0.000015 | 0.073100 | 0.282716 | 0.0 | 0.5 | 0.79 | 1.16 |
| BSS-8-17 | 0.002577 | 0.282675 | 0.000013 | 0.063368 | 0.282671 | −1.6 | 0.5 | 0.85 | 1.26 |
| BSS-8-18 | 0.002595 | 0.282687 | 0.000011 | 0.067361 | 0.282683 | −1.2 | 0.4 | 0.84 | 1.23 |
| *Jingangshan: 12JGS-5* | | | | | | | | | |
| 12JGS-5-01 | 0.003228 | 0.282662 | 0.000026 | 0.080005 | 0.282657 | −2.2 | 0.9 | 0.89 | 1.29 |
| 12JGS-5-02 | 0.003210 | 0.282696 | 0.000016 | 0.079064 | 0.282691 | −1.0 | 0.6 | 0.84 | 1.21 |
| 12JGS-5-04 | 0.003057 | 0.282691 | 0.000025 | 0.080851 | 0.282686 | −1.2 | 0.9 | 0.84 | 1.23 |
| 12JGS-5-05 | 0.001661 | 0.282670 | 0.000030 | 0.044493 | 0.282667 | −1.8 | 1.1 | 0.84 | 1.27 |
| 12JGS-5-06 | 0.001956 | 0.282678 | 0.000023 | 0.056648 | 0.282675 | −1.5 | 0.8 | 0.83 | 1.25 |
| 12JGS-5-07 | 0.002576 | 0.282697 | 0.000016 | 0.068817 | 0.282693 | −0.9 | 0.6 | 0.82 | 1.21 |
| 12JGS-5-08 | 0.002496 | 0.282712 | 0.000014 | 0.066324 | 0.282708 | −0.4 | 0.5 | 0.80 | 1.18 |
| 12JGS-5-09 | 0.002219 | 0.282635 | 0.000019 | 0.054064 | 0.282631 | −3.1 | 0.7 | 0.90 | 1.35 |
| 12JGS-5-10 | 0.002440 | 0.282608 | 0.000035 | 0.061541 | 0.282605 | −4.0 | 1.2 | 0.95 | 1.41 |
| 12JGS-5-11 | 0.002528 | 0.282699 | 0.000011 | 0.065732 | 0.282695 | −0.8 | 0.4 | 0.82 | 1.21 |
| 12JGS-5-12 | 0.001546 | 0.282726 | 0.000016 | 0.039420 | 0.282723 | 0.2 | 0.6 | 0.76 | 1.14 |
| 12JGS-5-13 | 0.003398 | 0.282710 | 0.000012 | 0.087474 | 0.282704 | −0.5 | 0.4 | 0.82 | 1.18 |
| 12JGS-5-14 | 0.004102 | 0.282727 | 0.000015 | 0.102920 | 0.282721 | 0.1 | 0.5 | 0.81 | 1.15 |
| 12JGS-5-15 | 0.003466 | 0.282735 | 0.000015 | 0.092952 | 0.282729 | 0.4 | 0.5 | 0.78 | 1.13 |
| 12JGS-5-16 | 0.002312 | 0.282689 | 0.000012 | 0.062179 | 0.282685 | −1.2 | 0.4 | 0.83 | 1.23 |
| 12JGS-5-17 | 0.003036 | 0.282735 | 0.000017 | 0.080807 | 0.282730 | 0.4 | 0.6 | 0.77 | 1.13 |
| 12JGS-5-18 | 0.002019 | 0.282695 | 0.000012 | 0.051750 | 0.282692 | −0.9 | 0.4 | 0.81 | 1.21 |
| 12JGS-5-19 | 0.001707 | 0.282707 | 0.000016 | 0.043949 | 0.282705 | −0.5 | 0.6 | 0.79 | 1.18 |
| 12JGS-5-20 | 0.002726 | 0.282706 | 0.000018 | 0.071391 | 0.282702 | −0.6 | 0.6 | 0.81 | 1.19 |
| *Wushan: 12WS-1* | | | | | | | | | |
| 12WS-1-01 | 0.001983 | 0.282672 | 0.000014 | 0.048396 | 0.282668 | −1.6 | 0.5 | 0.84 | 1.26 |
| 12WS-1-02 | 0.000755 | 0.282674 | 0.000015 | 0.018426 | 0.282673 | −1.5 | 0.5 | 0.81 | 1.25 |
| 12WS-1-03 | 0.002248 | 0.282671 | 0.000019 | 0.056200 | 0.282667 | −1.7 | 0.7 | 0.85 | 1.27 |
| 12WS-1-04 | 0.001350 | 0.282664 | 0.000017 | 0.034985 | 0.282662 | −1.9 | 0.6 | 0.84 | 1.28 |
| 12WS-1-05 | 0.003173 | 0.282691 | 0.000022 | 0.078426 | 0.282686 | −1.0 | 0.8 | 0.84 | 1.22 |
| 12WS-1-07 | 0.003576 | 0.282724 | 0.000019 | 0.102674 | 0.282718 | 0.1 | 0.7 | 0.80 | 1.15 |
| 12WS-1-08 | 0.001601 | 0.282682 | 0.000014 | 0.043415 | 0.282679 | −1.3 | 0.5 | 0.82 | 1.24 |
| 12WS-1-09 | 0.001223 | 0.282686 | 0.000014 | 0.031017 | 0.282684 | −1.1 | 0.5 | 0.81 | 1.23 |
| 12WS-1-10 | 0.001619 | 0.282652 | 0.000012 | 0.039407 | 0.282650 | −2.3 | 0.4 | 0.86 | 1.30 |
| 12WS-1-11 | 0.000597 | 0.282702 | 0.000011 | 0.014600 | 0.282701 | −0.5 | 0.4 | 0.77 | 1.19 |
| 12WS-1-12 | 0.002311 | 0.282684 | 0.000013 | 0.054692 | 0.282680 | −1.2 | 0.5 | 0.83 | 1.24 |
| 12WS-1-13 | 0.001023 | 0.282686 | 0.000013 | 0.025214 | 0.282684 | −1.1 | 0.4 | 0.80 | 1.23 |
| 12WS-1-14 | 0.001318 | 0.282697 | 0.000016 | 0.035753 | 0.282695 | −0.7 | 0.6 | 0.79 | 1.20 |

**Table 4** (*continued*)

| Spot | $^{176}Lu/^{177}Hf$ | $^{176}Hf/^{177}Hf$ | $2\sigma$ | $^{176}Yb/^{177}Hf$ | $(^{176}Hf/^{177}Hf)_i$ | $\varepsilon_{Hf}(t)$ | $2\sigma$ | $T_{DM1}$ (Ga) | $T_{DM2}$ (Ga) |
|---|---|---|---|---|---|---|---|---|---|
| 12WS-1-15 | 0.002275 | 0.282676 | 0.000011 | 0.058748 | 0.282672 | −1.5 | 0.4 | 0.84 | 1.25 |
| 12WS-1-16 | 0.001482 | 0.282624 | 0.000014 | 0.037669 | 0.282622 | −3.3 | 0.5 | 0.90 | 1.37 |
| 12WS-1-17 | 0.003085 | 0.282642 | 0.000018 | 0.074763 | 0.282637 | −2.8 | 0.6 | 0.91 | 1.33 |
| 12WS-1-18 | 0.001321 | 0.282641 | 0.000015 | 0.035210 | 0.282639 | −2.7 | 0.5 | 0.87 | 1.33 |
| 12WS-1-19 | 0.000881 | 0.282654 | 0.000017 | 0.022184 | 0.282652 | −2.2 | 0.6 | 0.84 | 1.30 |
| 12WS-1-20 | 0.001672 | 0.282716 | 0.000013 | 0.040055 | 0.282713 | −0.1 | 0.4 | 0.77 | 1.16 |
| 12WS-1-21 | 0.001028 | 0.282673 | 0.000014 | 0.026747 | 0.282672 | −1.5 | 0.5 | 0.82 | 1.25 |
| 12WS-1-22 | 0.002446 | 0.282696 | 0.000014 | 0.061741 | 0.282692 | −0.8 | 0.5 | 0.82 | 1.21 |
| 12WS-1-23 | 0.000879 | 0.282680 | 0.000016 | 0.022368 | 0.282679 | −1.3 | 0.6 | 0.81 | 1.24 |
| *Wushan: 12WS-1* | | | | | | | | | |
| 12WS-4-01 | 0.001011 | 0.282693 | 0.000016 | 0.024968 | 0.282691 | −0.9 | 0.6 | 0.79 | 1.21 |
| 12WS-4-02 | 0.001674 | 0.282708 | 0.000013 | 0.040811 | 0.282705 | −0.4 | 0.5 | 0.79 | 1.18 |
| 12WS-4-03 | 0.002654 | 0.282679 | 0.000012 | 0.063374 | 0.282674 | −1.4 | 0.4 | 0.85 | 1.25 |
| 12WS-4-04 | 0.001109 | 0.282688 | 0.000016 | 0.028659 | 0.282686 | −1.0 | 0.6 | 0.80 | 1.22 |
| 12WS-4-05 | 0.002279 | 0.282671 | 0.000010 | 0.053033 | 0.282667 | −1.7 | 0.3 | 0.85 | 1.27 |
| 12WS-4-06 | 0.002530 | 0.282657 | 0.000011 | 0.058230 | 0.282653 | −2.2 | 0.4 | 0.88 | 1.30 |
| 12WS-4-07 | 0.001674 | 0.282653 | 0.000013 | 0.042130 | 0.282650 | −2.3 | 0.5 | 0.86 | 1.30 |
| 12WS-4-08 | 0.001315 | 0.282634 | 0.000016 | 0.031340 | 0.282631 | −3.0 | 0.6 | 0.88 | 1.35 |
| 12WS-4-09 | 0.000811 | 0.282684 | 0.000014 | 0.019217 | 0.282682 | −1.2 | 0.5 | 0.80 | 1.23 |
| 12WS-4-10 | 0.002044 | 0.282695 | 0.000016 | 0.054155 | 0.282691 | −0.8 | 0.6 | 0.81 | 1.21 |
| 12WS-4-11 | 0.002174 | 0.282677 | 0.000019 | 0.058905 | 0.282673 | −1.5 | 0.7 | 0.84 | 1.25 |
| 12WS-4-12 | 0.001505 | 0.282676 | 0.000020 | 0.039321 | 0.282673 | −1.5 | 0.7 | 0.83 | 1.25 |
| 12WS-4-13 | 0.001309 | 0.282670 | 0.000019 | 0.032512 | 0.282668 | −1.7 | 0.7 | 0.83 | 1.26 |
| 12WS-4-14 | 0.001561 | 0.282694 | 0.000014 | 0.037650 | 0.282691 | −0.8 | 0.5 | 0.80 | 1.21 |
| 12WS-4-15 | 0.001318 | 0.282687 | 0.000014 | 0.033172 | 0.282685 | −1.1 | 0.5 | 0.81 | 1.22 |
| 12WS-4-16 | 0.001707 | 0.282694 | 0.000017 | 0.043837 | 0.282691 | −0.9 | 0.6 | 0.81 | 1.21 |
| 12WS-4-17 | 0.002310 | 0.282751 | 0.000015 | 0.064014 | 0.282747 | 1.1 | 0.5 | 0.74 | 1.08 |
| 12WS-4-18 | 0.002205 | 0.282648 | 0.000014 | 0.054482 | 0.282644 | −2.5 | 0.5 | 0.88 | 1.32 |
| 12WS-4-19 | 0.001237 | 0.282642 | 0.000019 | 0.030670 | 0.282639 | −2.7 | 0.7 | 0.87 | 1.33 |
| 12WS-4-20 | 0.001675 | 0.282680 | 0.000014 | 0.041883 | 0.282677 | −1.3 | 0.5 | 0.82 | 1.24 |
| 12WS-4-21 | 0.000916 | 0.282641 | 0.000018 | 0.022468 | 0.282639 | −2.7 | 0.6 | 0.86 | 1.33 |
| 12WS-4-22 | 0.000928 | 0.282653 | 0.000013 | 0.021867 | 0.282651 | −2.3 | 0.4 | 0.85 | 1.30 |

Note: $\varepsilon_{Hf}(t) = \{[(^{176}Hf/^{177}Hf)_s - (^{176}Lu/^{177}Hf)_s \times (e^{\lambda t} - 1)]/[(^{176}Hf/^{177}Hf)_{CHUR,0} - (^{176}Lu/^{177}Hf)_{CHUR,0} \times (e^{\lambda t} - 1)] - 1\} \times 10000$.
$T_{DM1} = 1/\lambda \times \ln\{1 + [(^{176}Hf/^{177}Hf)_s - (^{176}Hf/^{177}Hf)_{DM}]/[(^{176}Lu/^{177}Hf)_s - (^{176}Lu/^{177}Hf)_{DM}]\}$.
$T_{DM2} = 1/\lambda \times \ln\{1 + [(^{176}Hf/^{177}Hf)_{s,t} - (^{176}Hf/^{177}Hf)_{DM,t}]/[(^{176}Lu/^{177}Hf)_{cc} - (^{176}Lu/^{177}Hf)_{DM}]\} + t$.
Data sources: $(^{176}Lu/^{177}Hf)_{CHUR,0} = 0.0332$ and $(^{176}Hf/^{177}Hf)_{CHUR,0} = 0.828772$ (Blichert-Toft and Albarède, 1997); $(^{176}Lu/^{177}Hf)_{DM} = 0.0384$ and $(^{176}Hf/^{177}Hf)_{DM} = 0.28325$ (Vervoort and Blichert-Toft, 1999); $(^{176}Lu/^{177}Hf)_{cc} = 0.015$(Griffin et al., 2000); $\lambda = 1.867 \times 10^{-11}$/year (Söderlund et al., 2004).

2.10–2.40 Ga) in eastern Cathaysia (Xu et al., 2007). However, as mentioned above, the Baishishan, Jingangshan, and Wushan granites show relatively young model ages (1.14–1.42 Ga) that do not coincide with the episodes of regional crustal generation. This indicates the three A-type plutons were unlikely originated via partial melting of Mesoproterozoic juvenile crust in the area.

Collins et al. (1982) and Clemens et al. (1986) suggested that the partial melting of a residual granulitic source in the lower crust, which was previously depleted by extraction of a hydrous I-type felsic melt, may result in the generation of some A-type granites. Coincidentally, in previous studies, a similar model was also invoked by Chen et al. (2000, 2004) to account for the genetic relationship between I- and A-type granites exposed in the southeastern coast of Fujian Province. However, the observed enrichments in LILEs (especially Th, Cs, U, and Rb), and the high $SiO_2$ and alkali contents in the investigated A-type granites, preclude their derivation from a depleted granulitic residue in the lower crust, although such a residual model could provide a reasonable explanation for the existence of strong Ba, Sr, Eu, P, and Ti depletions in the A-type granites and the occurrence of the ca. 5-Myr intervals between spatially coexisting I- and A-type granites in coastal Fujian Province (Chen et al., 2000, 2013; Qiu et al., 2004). Experimental work has also suggested that the remelting of these residues cannot produce granitic magma with A-type geochemical signatures, for example, high $(Na_2O + K_2O)/Al_2O_3$ and $TiO_2/MgO$ ratios (Patiño Douce, 1997). More importantly, the Palaeoproterozoic was the main period of crustal growth in eastern Cathaysia (Chen and Jahn, 1998; Shen et al., 1993). Magmas generated by the partial melting of lower-crustal granulitic residues, from which the acid end-member component of the coexisting I-type granitoids was previously extracted, are expected to have similar Nd isotopic compositions to those of the basement rocks. However, this proposal is inconsistent with our isotopic data for the A-type granites in the present study (Fig. 8). Therefore, the remelting of a residual source from the lower crust is unlikely to produce the A-type magmas.

Creaser et al. (1991) systematically suggested that the partial melting of crustal magmatic rocks with tonalitic or granodioritic compositions may generate granitic magmas with A-type affinities. This viewpoint was corroborated by subsequent experimental studies (Patiño Douce, 1997; Skjerlie and Johnston, 1993), although it was emphasized that low-pressure conditions are another key factor controlling the generation of high-silica aluminous A-type granites, in addition to source composition. King et al. (1997) proposed that aluminous A-type granites were likely derived from the high-temperature partial melting of a felsic infracrustal source. Field investigations show that the studied A-type granites intruded the Zhangpu I-type granitoids, forming a composite batholith. They show similar Nd isotopic compositions to those of the I-type granitoids from Zhangpu and adjacent areas (Fig. 8), suggesting that the pre-existing I-type calc-alkaline granitoids can provide a suitable protolith for the studied A-type granites. Moreover, ratios between LILEs and HFSEs (e.g., Rb/Nb, Th/Ta, and La/Ta) are slightly higher in the A-type granites than in the I-type granitoids from Zhangpu and adjacent areas. This also provides support for our speculation, because LILEs are generally more incompatible than HFSEs during crustal melting, and thus melts generated by the partial melting of crustal rocks preserve or increase LILE/HFSE ratios (Barboni and

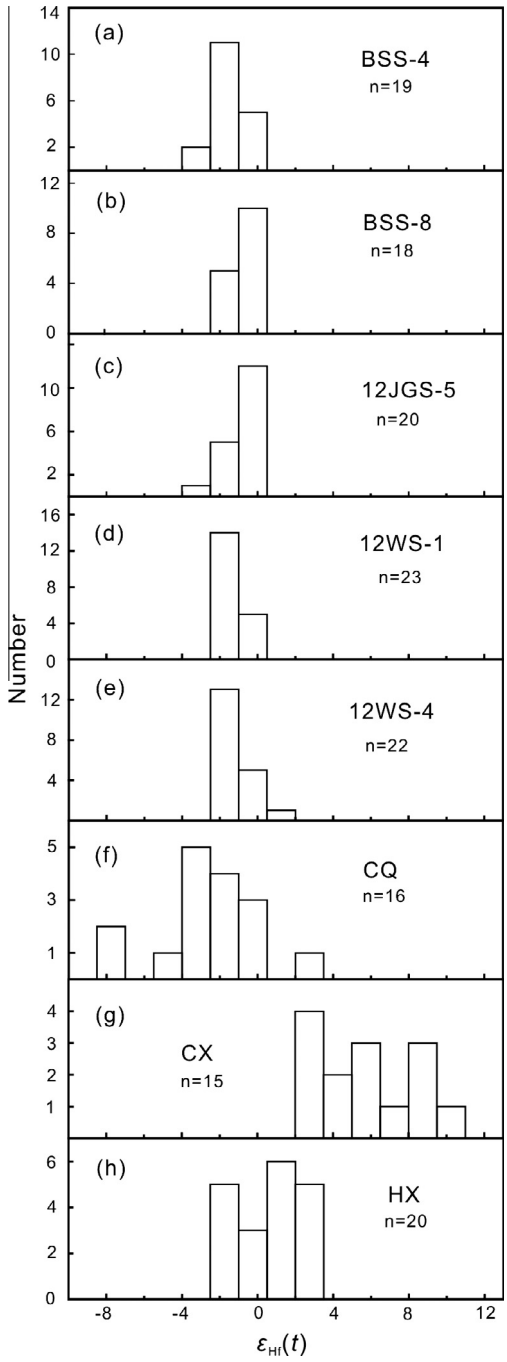


**Fig. 9.** Histogram of $\varepsilon_{Hf}(t)$ values of zircons from Baishishan (a and b), Jingangshan (c), Wushan (d and e) and related Zhangpu composite granite pluton (including Changqiao (f), Chengxi (g) and Huxi (h) intrusions). The data of Zhangpu composite granite pluton are from Qiu et al. (2012).

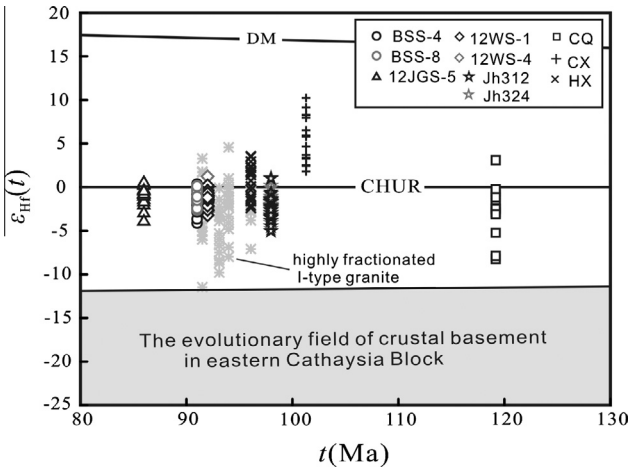


**Fig. 10.** Diagram of $\varepsilon_{Hf}(t)$ values *vs.* U–Pb ages for zircons from A- and I-type granitic rocks in the southeast coast of Fujian Province. The Hf isotopic evolutionary area shown for the crustal basement of the Cathaysia Block is after Xu et al. (2007). Data of the Changqiao (CQ), Chenxi (CX) and Huxi (HX) granites are from Qiu et al. (2012), and those of Xincun granite (Jh312, Jh324) are from Chen et al. (2013). Data of highly fractionated I-type granites are from Qiu et al. (2008). DM – depleted mantle; CHUR – chondritic uniform reservoir.

Bussy, 2013; Beard et al., 1994). More recently, Frost and Frost (2011) suggested that such aluminous A-type granites formed by the partial melting of tonalitic or granodioritic sources should be high-silica, calc-alkalic rocks. The silica-enriched, calc-alkalic signatures of the aluminous A-type granites in the Baishishan, Jingangshan, and Wushan plutons indicate that their formation was most likely related to partial melting of a tonalitic to granodioritic source. More importantly, the granites in the three plutons are compositionally characterized by relatively high total alkali contents and NK/A ratios, low A/CNK ratios, and depletion in both $Al_2O_3$ and CaO, which is in agreement with the compositions of experimental melts produced by the melting of tonalite and granodiorite at 950 °C and 4 kbar (Fig. 6c and d, Patiño Douce, 1997), implying their derivation from a tonalitic to granodioritic source. In summary, we propose that the Baishishan, Jingangshan, and Wushan aluminous A-type granites were generated by the partial melting of pre-existing I-type calc-alkaline granitoids. Such a genetic relationship between aluminous A-type and I-type granitoids has been widely reported in many previous studies (e.g., Farahat et al., 2007; Chen et al., 2013).

### 6.3. An integrated petrogenetic model

To examine our assumptions regarding the generation of the investigated A-type granites via the partial melting of a tonalitic or granodioritic magma source, a non-modal partial melting simulation was conducted using the least evolved granodiorite sample from the Huxi intrusion as a source (Qiu et al., 2012). The modal mineralogical composition of the source rocks was taken to be 25% quartz, 45% plagioclase, 15% K-feldspar, 5% amphibole, and 10% biotite. The calculated compositions of the melts produced by 40%, 50%, and 60% partial melting, together with the calculation procedure and related parameters used for modelling the trace elements (Rb, Ba, K, Sr, and Nb) are given in Table 5. The obtained results indicate that the Rb, K, and Nb concentrations of the investigated A-type granites could be well reproduced by high degrees of batch partial melting (Table 5), whereas the calculated Ba and Sr abundances are distinctly higher than the values observed in the studied A-type granites. Considering the possible crystal fractionation of plagioclase, biotite, and K-feldspar during magma evolution, the relatively high simulation values for Ba and Sr may be considered reasonable. The simulation results also suggest that the A-type granites can be formed by high degrees of partial melting of tonalitic or granodioritic sources. However, whether the generation of these A-type granites was related to the Huxi granodiorite still requires further investigation.

The Baishishan, Jingangshan, and Wushan granites show relatively high HREE contents and flat HREE patterns, which argues for the absence of garnet in residual phases (Mushkin et al., 2003). In addition, the granites commonly show intensive depletion of Sr,

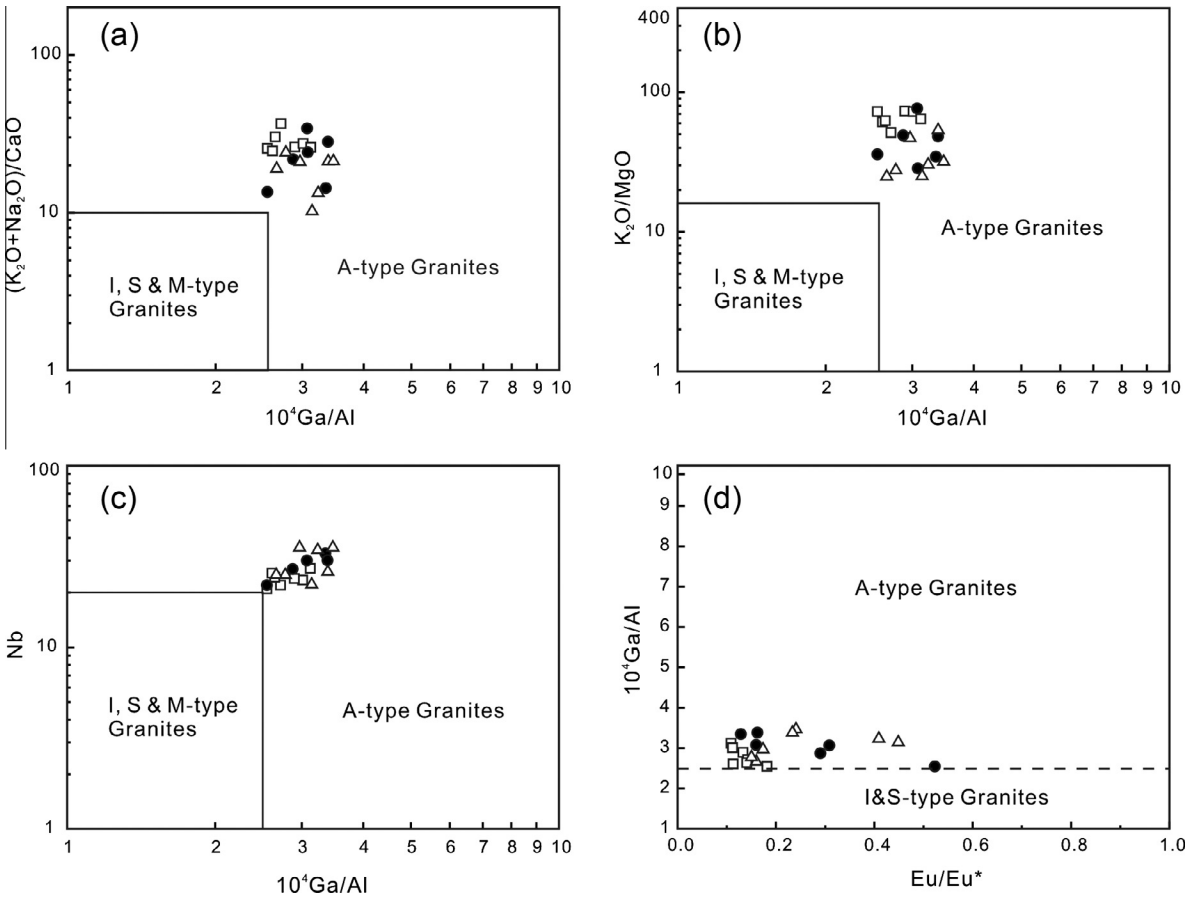


**Fig. 11.** Various chemical discrimination diagrams for Baishishan, Jingangshan and Wushan granites. Base maps of (a), (b) and (c) are after Whalen et al. (1987), and (d) is after Eby (1992). Part of the data for Jingangshan and Wushan granites are from Hong et al. (1987) and Qiu et al. (2004), respectively, Symbols are the same as those in Fig. 6.

**Table 5**
Simulation results of trace elements using non-modal partial melting model.

| | Source | $D_0$ | $P$ | Calculated melt | | | Measured melt |
|---|---|---|---|---|---|---|---|
| | | | | $F = 0.4$ | $F = 0.5$ | $F = 0.6$ | |
| Rb (ppm) | 128.7 | 0.31 | 0.45 | 243 | 220 | 201 | 169–381 |
| Sr (ppm) | 411.2 | 2.57 | 2.53 | 209 | 227 | 248 | 4–118 |
| Ba (ppm) | 1175.4 | 1.72 | 2.62 | 1091 | 1284 | 1559 | 15–539 |
| $K_2O$ (wt.%) | 3.14 | 0.45 | 0.62 | 5.22 | 4.92 | 4.64 | 4.67–3.88 |
| Nb (ppm) | 16.58 | 0.89 | 1.21 | 21 | 21 | 22 | 22–35 |

Mineral/melt partition coefficients are from Rollinson (1993), Philpotts and Schnetzler (1970), Ewart and Griffin (1994) and GERM (Geochemical Earth Reference Model; http://www.earthref.org/GERM). Equation for the non-modal batch partial melting is $C_L = C_0/[D_0 + F(1 - P)]$ (Shaw, 1970), where $C_L$ and $C_0$ are the concentration of a trace element in the melt and in the source, respectively, $F$ represents the melt fraction, $D_0$ is the bulk distribution coefficient for the starting assemblage, and $P$ is the bulk distribution coefficient of the minerals that make up the melt.

strongly negative Eu anomalies, and high Rb/Sr ratios, even in the least evolved sample (12WS-3). These characteristics imply that the partial melting of source rocks likely took place within the stability field of plagioclase, further pointing to a shallow source depth. Some elemental variations (e.g., $SiO_2$ *vs.* $Na_2O + CaO$ and Sr *vs.* Ba; Fig. 12a and b) imply that the primary magma generated from the partial melting of a granodioritic source subsequently underwent further fractionation of plagioclase and K-feldspar. These results lead us to further conclude that the investigated A-type granites were produced by the dehydration melting of hornblende- and biotite-bearing granitoids, with plagioclase-rich residual phases in the middle to lower crust, followed by variable degrees of differentiation.

The origin and geodynamic mechanism of the widespread Late Mesozoic magmatic rocks in SE China is an important topic of international research interest. Despite some controversy, a growing number of researchers consider that Cretaceous magmatism along the coastal area of SE China was formed in an active continental margin due to subduction of the Palaeo-Pacific plate (Chen et al., 2008; Li et al., 2007; Li and Li, 2007; Zhou et al., 2006). The Baishishan, Jingangshan, and Wushan granites were emplaced during the Late Cretaceous (92–86 Ma), and are nearly contemporaneous with other A-type granites in the region (101–92 Ma; Lin et al., 2011; Qiu et al., 1999a, 2004; Xiao et al., 2007), suggesting a wide back-arc extensional setting in the coastal region of SE China. In addition, numerous lines of geochemical and geological evidence also demonstrate that Cretaceous I-type granites in the Fujian coastal area formed in an extensional tectonic environment (Jiang et al., 2011; Li et al., 2014; Wong et al., 2009). These observations indicate that the intimately associated A- and I-type granites were produced in the same extensional tectonic setting, despite the fact that they had distinct sources and were formed by different processes. It is worth noting that large amounts of extension-related rocks in the coastal areas of Zhejiang and Fujian Provinces, such as A-type granites, bimodal volcanic rock associations (101–83 Ma; Chen et al., 2008; Qiu et al., 1999b; Zhou et al., 1994), and basic dikes (96–84 Ma; Dong et al., 2011; Qin et al., 2010; Yang et al., 2010; Zhang et al., 2007), were

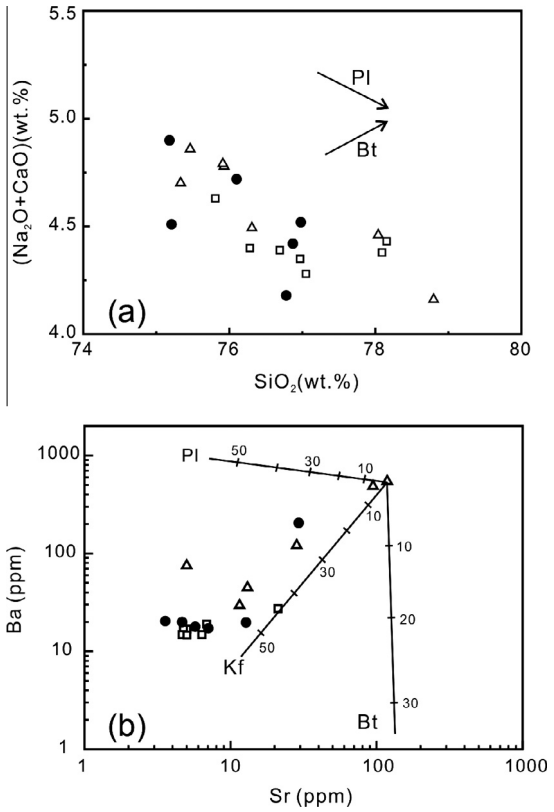


**Fig. 12.** (a) $SiO_2$ *vs.* $Na_2O + CaO$, (b) Sr *vs.* Ba diagrams, showing that fractional crystallization of plagioclase, biotite and K-feldspar plays an important role in the generation of the Baishishan, Jingangshan and Wushan granites. Partition coefficients of Ba and Sr are from Arth (1976) for plagioclase and K-feldspar, and from Philpotts and Schnetzler (1970) for biotite. Pl: plagioclase; Kf: K-feldspar; Bt: biotite. Symbols are the same as those in Fig. 6.

developed during a narrow time interval of 101–83 Ma, indicating a peak in regional lithospheric extension during the Late Cretaceous in response to rollback of the Palaeo-Pacific plate, as suggested by Jiang et al. (2011) and Li et al. (2014). Thus, gradually intensifying regional extension in the coastal region of SE China may have been a major dynamic mechanism responsible for the emplacement of I-type granites (122–96 Ma; Li et al., 2014) and subsequently A-type granites (92–86 Ma) in the Zhangpu region.

Tectonically, the emplacement of the Baishishan, Jingangshan, and Wushan A-type granitic plutons, as well as the associated Zhangpu I-type composite granite pluton, were along the NE–NNE-trending Changle–Nan'ao Fault, which is commonly considered to be a transcrustal sinistral fault associated with multi-stage ductile deformation and metamorphism (Chen et al., 2002; Shu et al., 2000). The key role of fault systems in the generation, ascent, and emplacement of granitic magmas has been emphasized by Abdel Rahman (2006) and Konopelko et al. (2007). It is notable that Cretaceous volcano–magmatic activity is widely distributed along the Changle–Nan'ao Fault, which is nearly parallel to the coastline of SE China, forming a nearly NNE-trending granitoid belt (Fig. 1). Such a distribution of the granitoids with nearly uniform emplacement ages, low Nd isotopic model ages (Chen and Jahn, 1998; Zhou et al., 2006), and similar geochemical characteristics may indicate their formation was triggered by tectonic factors rather than local crustal melting. A series of studies have suggested that the generation of granitoids in coastal Fujian and Zhejiang provinces is not directly related to subduction of the Palaeo-Pacific plate but more likely to activity of the Changle–Nan'ao Fault, which may have been a potential channel for the underplating of mantle-derived mafic magmas (Martin et al., 1994; Zhou et al., 2006). Consequently, extensional activation of the Changle–Nan'ao Fault may play an important role in the derivation of regional granitoids.

Based on this review of the data, we propose an integrated model to explain the generation of A-type and coexisting I-type granitoids, as shown schematically in Fig. 13. From the early stage of regional extension (~125 Ma; Li et al., 2014), underplating of mantle-derived basaltic magmas resulted in the large-scale partial melting of lower-crustal materials that produced felsic magmas. These magmas then mixed extensively with mantle-derived mafic magmas, thus generating the I-type granitic magma in the Zhangpu area. During this process, some I-type hybrid magma might have been stranded in the middle–lower crust, forming a localized A-type source region that was separated vertically from other granite sources in the region (Fig. 13a). Subsequently, ongoing lithospheric extension and crustal attenuation, especially during the Late Cretaceous, induced more intensive underplating of the mantle-derived mafic magma. The shearing and extension enabled the fault planes of regional faults to propagate to greater depths and resulted in opening of the fault zones. Thus, the fault systems likely provided a suitable conduit for ascending mantle-derived melts, and resulted in the influx of heat into the crust. In this scenario, the uninterrupted underplated magma migrated upward, crossing the fault and reaching the middle–lower crust. The ascent of mafic magma triggered decompression melting of the overlying middle–lower crustal tonalitic–granodioritic source rocks to produce the A-type parental magmas (Fig. 13b). After further removal of plagioclase and K-feldspar, the remaining melt was emplaced in relatively shallow crust as a result of lithospheric extension, and finally formed the Baishishan, Jingangshan, and Wushan plutons.

## 7. Conclusions

(1) The granites from the Baishishan, Jingangshan, and Wushan plutons share common petrographic and geochemical features. Geochemically, they belong to a metaluminous to slightly peraluminous high-K calc-alkaline series and are characterized by high contents of $SiO_2$ and $K_2O + Na_2O$, high Ga/Al, $FeO^{tot}/MgO$, and $(K_2O + Na_2O)/CaO$ ratios, enrichments in some LILEs (e.g., Cs, K, U, and Th) and HFSEs (e.g., Nb and Ta), and significant depletions in Ba, Sr, P, Ti, and Eu, and show aluminous A-type affinities.

(2) Petrographic, geochemical, and Nd–Hf isotopic studies, together with constraints from experimental petrology, suggest that the Baishishan, Jingangshan, and Wushan granites were likely derived from a tonalitic to granodioritic source with plagioclase residual phases at middle–lower crustal levels, coupled with further differentiation during their ascent and emplacement. Accordingly, the pre-existing I-type calc-alkaline granitoids provided a suitable protolith for the investigated aluminous A-type granites, based on their close genetic relationship.

(3) The zircon U–Pb dating results indicate that the Baishishan, Jingangshan, and Wushan granites were emplaced at 92–86 Ma, which is slightly younger than the I-type granitoids in the Zhangpu region (122–96 Ma), but coeval with the A-type granites, bimodal volcanic rock associations, and mafic dykes exposed in the coastal area of Zhejiang and Fujian Provinces, SE China. These observations suggest a gradual intensification of regional extension in SE China during the late Yanshanian. The induced underplating of mantle-derived magma was probably the heat source for the generation of regional granitic rocks, regardless of whether they were A-type or I-type granites. Continuous Cretaceous

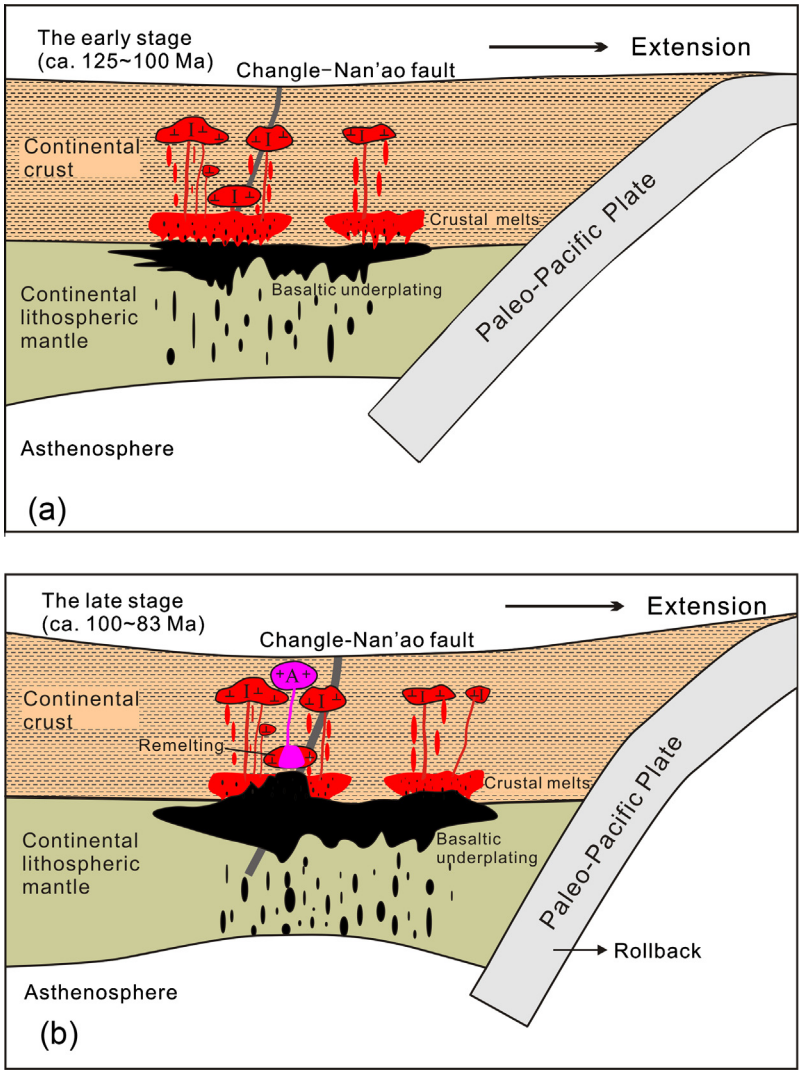


**Fig. 13.** Schematic cartoon showing the generation and emplacement of the A-type and I-type granites in the southeast Fujian Province, South China (modified after He et al., 2010; Liu et al., 2013).

lithospheric extension and possible activation of deep faults related to the subduction of the Palaeo-Pacific plate may have exerted a significant role in the origin of I-type granites (122–96 Ma) and subsequently A-type granites.

## Acknowledgements

We are thankful to the Western Geological Party of Fujian Province for assisting with fieldwork and sample collection, and to Ms. W. Pu for her assistance with Nd isotope analysis, and to Prof. Jin-Cheng Zhou for his help in preparation the early draft of this manuscript. We also thank two anonymous reviewers for their thoughtful comments and constructive suggestions which greatly improved the manuscript. This study was financially supported by the National 973 Project of the Chinese Ministry of Science and Technology (grant no. 2012CB416702), and the Specialized Research Fund for the Doctoral Program of Higher Education of China (grant no. 20120091130003).

## References

Abdel Rahman, A.M., 2006. Petrogenesis of anorogenic peralkaline granitic complexes from eastern Egypt. Mineral. Mag. 70, 27–50.

Andersen, T., 2002. Correction of common lead in U–Pb analyses that do not report $^{204}$Pb. Chem. Geol. 192, 59–79.

Arth, J.G., 1976. Behavior of trace elements during magmatic processes – a summary of theoretical models and their applications. J. Res. U.S. Geol. Surv. 4, 41–47.

Barboni, M., Bussy, F., 2013. Petrogenesis of magmatic albite granites associated to cogenetic A-type granites: Na-rich residual melt extraction from a partially crystallized A-type granite mush. Lithos 177, 328–351.

Beard, J.S., Lofgren, G.E., Sinha, A.K., Tollo, R.P., 1994. Partial melting of apatite-bearing charnockite, granulite, and diorite: melt composition, restite mineralogy, and petrologic implications. J. Geophys. Res. 99, 21591–21603.

Belousova, E.A., Griffin, W.L., O'reilly, S.Y., 2006. Zircon crystal morphology, trace element signatures and Hf isotope composition as a tool for petrogenetic modeling: examples from Eastern Australian granitoids. J. Petrol. 47, 329–353.

Black, L.P., Gulson, B.L., 1978. The age of the mud tank carbonatite, Strangways range, Northern territory. BMR J. Aust. Geol. Geophys. 3, 227–232.

Blichert-Toft, J., Albarède, F., 1997. The Lu–Hf geochemistry of chondrites and evolution of the mantle-crust system. Earth Planet. Sci. Lett. 148 (1–2), 243–258.

Bonin, B., 2007. A-type granites and related rocks: evolution of a concept, problems and prospects. Lithos 97 (1–2), 1–2.

Boynton, W.V., 1984. Geochemistry of the rare earth elements: meteorite studies. In: Henderson, P. (Ed.), Rare Earth Elements Geochemistry. Elsevier, Amsterdam, pp. 63–144.

Chappell, B.W., 1999. Aluminium saturation in I- and S-type granites and the characterization of fractionated haplogranites. Lithos 46, 535–551.

Chen, J.F., Jahn, B., 1998. Crustal evolution of southeastern China: Nd and Sr isotopic evidence. Tectonophysics 284, 101–133.

Chen, C.H., Lin, W., Lee, C.Y., Tien, J.L., Lu, H.Y., Lai, Y.H., 2000. Cretaceous fractionated I–type granitoids and metaluminous A-type granites in SE China: the Late Yanshanian post-orogenic magmatism. Trans. Roy. Soc. Edin.: Earth Sci. 91, 195–205.

Chen, W.S., Yang, H.C., Wang, X., Huang, H., 2002. Tectonic setting and exhumation history of the Pingtan–Dongshan Metamorphic Belt along the coastal area, Fujian Province, Southern China. J. Asian Earth Sci. 20, 829–840.
Chen, C.H., Lin, W., Lan, C.Y., Lee, C.Y., 2004. Geochemical and Sr, Nd isotopic characteristics and tectonic implications for three stages of igneous rock in the Late Yanshanian (Cretaceous) orogeny, SE China. Trans. Roy. Soc. Edin.: Earth Sci. 95, 237–248.
Chen, C.H., Lee, C.Y., Lu, H.Y., Hsieh, P.S., 2008. Generation of late Cretaceous silicic rocks in SE China: age, major element and numerical simulation constraints. J. Asian Earth Sci. 31, 479–498.
Chen, J.Y., Yang, J.H., Zhang, J.H., Sun, J.F., Wilde, S.A., 2013. Petrogenesis of the Cretaceous Zhangzhou batholith in southeastern China: zircon U–Pb age and Sr–Nd–Hf–O isotopic evidence. Lithos 162–163, 140–156.
Clemens, J., Holloway, J.R., White, A., 1986. Origin of an A-type granite: experimental constraints. Am. Mineral. 71, 317–324.
Collins, W.J., Beams, S.D., White, A.J.R., Chappell, B.W., 1982. Nature and origin of A-type granites with particular reference to southeastern Australia. Contrib. Mineral. Petrol. 80, 189–200.
Creaser, R.A., Price, R.C., Wormald, R.J., 1991. A-type granites revisited: assessment of a residual-source modal. Geology 19, 163–166.
Dahlquist, J.A., Alasino, P.H., Eby, G.N., Galindo, C., Casquet, C., 2010. Fault controlled Carboniferous A-type magmatism in the proto-Andean foreland (Sierras Pampeanas, Argentina): geochemical constraints and petrogenesis. Lithos 115, 65–81.
Dong, C.W., Peng, Y.M., 1994. Qingtian composite body—the coexisting of two different types of granites. J. Zhejiang Univ.: Nat. Sci. 28 (4), 440–448 (in Chinese with English abstract).
Dong, C.W., Zhang, D.R., Xu, X.S., Yan, Q., Zhu, G.Q., 2006. SHRIMP U–Pb dating and lithogeochemistry of basic-intermediate dike swarms from Jinjiang, Fujian Province. Acta Petrol. Sinica 22 (60), 1696–1702.
Dong, C.W., Zhou, C., Gu, H.Y., Ma, X.X., LÜ, Q., 2011. The age difference, geochemistry and petrogenesis of mafic dikes and host granites from Meizhou island in Fujian Province. J. Jilin Univ.: Earth Sci. Ed. 41 (3), 735–744 (in Chinese with English abstract).
Eby, G.N., 1990. A-type granitoids: a review of their occurrence and chemical characteristics and speculations on their petrogenesis. Lithos 26, 115–134.
Eby, G.N., 1992. Chemical subdivision of the A-type granitoids: petrogenetic and tectonic implications. Geology 20, 641–644.
Ewart, A., Griffin, W.L., 1994. Application of proton-microprobe data to trace-element partitioning in volcanic-rocks. Chem. Geol. 117 (1–4), 251–284.
Farahat, E.S., Mohamed, H.A., Ahmed, A.F., Mahallawi, M.M.E., 2007. Origin of I- and A-type granitoids from the Eastern Desert of Egypt: IMPLICATIONS for crustal growth in the northern Arabian-Nubian Shield. J. Afr. Earth Sc. 49, 43–58.
Frost, C.D., Frost, B.R., 2011. On ferroan (A-type) granitoids: their compositional variability and modes of origin. J. Petrol. 52 (1), 39–53.
Frost, B.R., Barnes, C.G., Collins, W.J., Arculus, R.J., Ellis, D.J., Frost, C.D., 2001. A geochemical classification for granitic rocks. J. Petrol. 42, 2033–2048.
Gao, J.F., Lu, J.J., Lin, Y.P., Pu, W., 2003. Analysis of trace elements in rock samples using HR-ICPMS. J. Nanjing Univ. (Nat. Sci.) 39, 844–850 (in Chinese with English abstract).
Green, T.H., 1995. Significance of Nb/Ta as an indicator of geochemical processes in the crust-mantle system. Chem. Geol. 120, 347–359.
Griffin, W.L., Pearson, N.J., Belousova, E., Jackson, S.E., van Achterbergh, E., O'Reilly, S.Y., Shee, S.R., 2000. The Hf isotope composition of cratonic mantle: LAM-MC-ICPMS analysis of zircon megacrysts in kimberlites. Geochim. Cosmochim. Acta 64 (1), 133–147.
Griffin, W.L., Wang, X., Jackson, S.E., Pearson, N.J., O'Reilly, S.Y., Xu, X.S., Zhou, X.M., 2002. Zircon chemistry and magma mixing, SE China: in-situ analysis of Hf isotopes, Tonglu and Pingtan igneous complexes. Lithos 61, 237–269.
Griffin, W.L., Pearson, N.J., Belousova, E.A., 2007. Reply to "Comment to short-communication 'Comment: Hf –isotope heterogeneity in zircon 91500' by W.L. Griffin, N.J. Pearson, E.A. Belousova and A. Saeed (Chemical geology 233 (2006) 358–363)" by F. Corfu. Chem. Geol. 244 (1–2), 354–356.
He, Z.Y., Xu, X.S., Niu, Y.L., 2010. Petrogenesis and tectonic significance of a Mesozoic granite-syenite-gabbro association from inland South China. Lithos 119, 621–641.
Hergt, J., Woodhead, J., Schofield, A., 2007. A-type magmatism in the Western Lachlan Fold Belt? A study of granites and rhyolites from the Grampians region, Western Victoria. Lithos 97, 122–139.
Hofmann, A.W., Jochum, K.P., Seufert, M., White, W.M., 1986. Nb and Pb in oceanic basalts: new constraints on mantle evolution. Earth Planet. Sci. Lett. 79, 33–45.
Hong, D.W., Guo, W.Q., Li, G.J., Kang, W., Xu, H.M., 1987. Petrology of the Miarolitic Granite Belt in the Southeast Coast of Fujian Province and their Petrogenesis. Science and Technology Press of Beijing, Beijing, pp. 92–94 (in Chinese with English abstract).
Jackson, S.E., Pearson, N.J., Griffin, W.L., Belousoval, E.A., 2004. The application of laser ablation–inductively coupled plasma–mass spectrometry (LA–ICP–MS) to in situ U–Pb zircon geochronology. Chem. Geol. 211, 47–69.
Jahn, B.M., Condie, K.C., 1995. Evolution of the Kaapvaal Craton as viewed from geochemical and Sm–Nd isotopic analyses of intracratonic pelites. Geochim. Cosmochim. Acta 59, 2239–2258.
Jiang, Y.H., Zhao, P., Zhou, Q., Liao, S.Y., Jin, G.D., 2011. Petrogenesis and tectonic implications of Early Cretaceous S-and A-type granites in the northwest of the Gan-Hang rift, SE China. Lithos 121, 55–73.
Karsli, O., Caran, Ş., Dokuz, A., Çoban, H., Chen, B., Kandermir, R., 2012. A-type granitoids from the Eastern Pontides, NE Turkey: records for generation of hybrid A-type rocks in a subduction-related environment. Tectonophysics 530–531, 208–224.
Kemp, A.I.S., Wormald, R.J., Whitehouse, M.J., Price, R.C., 2005. Hf isotopes in zircon reveal contrasting sources and crystallization histories for alkaline to peralkaline granites of Temora, southeastern Australia. Geology 33 (10), 797–800.
King, P.L., White, A.J.R., Chappell, B.W., Allen, C.M., 1997. Characterization and origin of aluminous A-type granites from the Lachlan Fold Belt, Southeastern Australia. J. Petrol. 38 (3), 371–391.
King, P.L., Chappell, B.W., Allen, C.M., White, A.J.R., 2001. Are A-type granites the high-temperature felsic granites? Evidence from fractionated granites of the Wangrah Suite. Aust. J. Earth Sci. 48, 501–514.
Konopelko, D., Biske, G., Seltmann, R., Eklund, O., Belyatsky, B., 2007. Hercynian post-collisional A-type granites of the Kokshaal Range, Southern Tien Shan, Kyrgyzstan. Lithos 97, 140–160.
Li, X.H., 1997. Timing of the Cathaysia Block formation: constraints from SHRIMP U–Pb zircon geochronology. Episodes 20, 188–192.
Li, Z.X., Li, X.H., 2007. Formation of the 1300 kn-wide intracontinental orogeny and post-orogenic magmatic province in Mesozoic South China: a flat-slab subduction model. Geology 35, 179–182.
Li, W.X., Li, X.H., Li, Z.X., 2005. Neproterozoic bimodal magmatism in the Cathaysia Block of South China and its tectonic significance. Precambr. Res. 136, 51–66.
Li, X.H., Li, Z.X., Li, W.X., Liu, Y., Yuan, C., Wei, G.J., Qi, C.S., 2007. U–Pb zircon, geochemical and Sr–Nd–Hf isotopic constraints on age and origin of Jurassic I- and A-type granites from central Guangdong, SE China: a major igneous event in response to foundering of a subducted flat-slab? Lithos 96 (1–2), 186–204.
Li, X.H., Long, W.G., Li, Q.L., Liu, Y., Zheng, Y.F., Yang, Y.H., Chamberlain, K.R., Wan, D.F., Guo, C.H., Wang, X.C., Tao, H., 2010. Penglai zircon megacrysts: a potential new working reference material for microbeam determination of Hf–O isotopes and U–Pb age. Geostand. Geoanal. Res. 34 (2), 117–134.
Li, L.L., Zhou, H.H., Chen, Z.H., Wang, J.R., Xiao, Y., 2011. Geochemical characteristics of granites in Taimushan area, Fujian Province, and their geological significance. Acta Petrol. Mineral. 30 (4), 593–609 (in Chinese with English abstract).
Li, Z., Qiu, J.S., Yang, X.M., 2014. A review of the geochronology and geochemistry of Late Yanshanian (Cretaceous) plutons along the Fujian coastal area of southeastern China: implications for magma evolution related to slab break-off and rollback in the Cretaceous. Earth Sci. Rev. 128, 232–248.
Lin, Q.C., Cheng, X.W., Zhang, Y.Q., Wang, F.Y., 2011. Evolution of granitoids in the active continental margin: a case study of the Fuzhou compound complex. Acta Geol. Sinica 85 (7), 1128–1133 (in Chinese with English abstract).
Liu, L., Qiu, J.S., Li, Z., 2013. Origin of mafic microgranular enclaves (MMEs) and their host quartz monzonites from the Muchen pluton in Zhejiang Province, Southeast China: implication for magma mixing and crust-mantle interaction. Lithos 160–161, 145–163.
Loiselle, M.C., Wones, D.R., 1979. Characteristics and origin of anorogenic granites. In: Abstracts Papers to be Presented at the Annual Meetings of the Geological Society of America and Associated Societies, San Diego, CA 11, p. 468.
Luding, K.R., 2001. Isoplot/Ex (rev. 2.49): a Geochronological Toolkit for Microsoft Excel: Berkeley Geochronology Center, Special Publication, 1, pp. 1–58.
Lugmair, G.W., Harti, K., 1978. Lunar initial $^{143}Nd/^{144}Nd$: differential evolution of the lunar crust and mantle. Earth Planet. Lett. 39, 349–357.
Manilar, P.D., Piccoli, P.M., 1989. Tectonic discrimination of granitoids. Geol. Soc. Am. Bull. 101, 635–643.
Martin, H., Bonin, B., Capdevila, R., Jahn, B.M., Lameyre, J., Wang, Y., 1994. The Kuiqi peralkaline granitic complex (SE China): petrology and geochemistry. J. Petrol. 35, 983–1015.
McDonough, W.F., Sun, S.S., 1995. The composition of the Earth. Chem. Geol. 120, 223–253.
Middlemost, E.A.K., 1985. Magma and Magmatic Rocks. Longman, London, 266pp.
Miller, R.G., O'Nions, R.K., 1985. Source of Precambrian chemical and clastic sediments. Nature 314, 325–330.
Mushkin, A., Navon, O., Halicz, L., Hartmann, G., Stein, M., 2003. The petrogenesis of A-type magmas from the Amram Massif, southern Israel. J. Petrol. 44, 815–832.
Nardi, L.V.S., Bitencourt, M.F., 2009. A-type granitic rocks in post-collisional settings in southernmost Brazil: their classification and relationship with tectonics and magmatic series. Can. Mineral. 47, 1493–1503.
Patiño Douce, A.E., 1997. Generation of metaluminous A-type granitoids by low-pressure melting of calc-alkaline granitoids. Geology 25, 743–746.
Peccerillo, A., Taylor, D.R., 1976. Geochemistry of Eocene calc-alkaline volcanic rocks from the Kaitamonu area, Northern Turkey. Contrib. Miner. Petrol. 58, 63–91.
Philpotts, J.A., Schnetzler, C.C., 1970. Phenocryst-matrix partition coefficients for K, Rb, Sr and Ba, with applications to anorthosite and basalt genesis. Geochim. Cosmochim. Acta 34, 307–322.
Poitrasson, F., Pin, C., Duthou, J.L., Platevoet, B., 1994. Aluminous subsolvus anorogenic granite genesis in the light of Nd isotopic heterogeneity. Chem. Geol. 112, 199–219.
Poitrasson, F., Duthou, J.L., Pin, C., 1995. The relationship between petrology and Nd isotopes as evidences for contrasting anorogenic granite genesis: example of the Corsican Province (SE France). J. Petrol. 36, 1251–1274.
Pu, W., Zhao, K.D., Ling, H.F., Jiang, S.Y., 2004. High precision Nd isotopes measurement by Triton TI Mass Spectrometry. Acta Geosci. Sinica 25, 271–274 (in Chinese with English abstract).
Pu, W., Gao, J.F., Zhao, K.D., Lin, H.F., Jiang, S.Y., 2005. Separation method of Rb–Sr, Sm–Nd using DCTA and HIBA. J. Nanjing Univ. (Nat. Sci.) 41, 445–450 (in Chinese with English abstract).

Qin, S.C., Fan, W.M., Guo, F., Li, C.W., Gao, X.F., 2010. Petrogenesis of late Mesozoic diabase dikes in Zhejiang–Fujian Provinces: constraints from $^{40}Ar$–$^{39}Ar$ and geochemistry. Acta Petrol. Sinica 26 (11), 3295–3306 (in Chinese with English abstract).

Qiu, J.S., Wang, D.Z., Mclnnes, B.I.A., 1999a. Geochemistry and petrogenesis of the I- and A- type composite granite masses in the coastal area of Zhejiang and Fujian Provinces. Acta Petrol. Sinica 15 (2), 237–246 (in Chinese with English abstract).

Qiu, J.S., Wang, D.Z., Zhou, J.C., 1999b. Geochemistry and petrogenesis of the late Mesozoic bimodal volcanic rocks at Yunshan caldera, Yongtai county, Fujian Province. Acta Petrol. Mineral. 18 (2), 97–107 (in Chinese with English abstract).

Qiu, J.S., Wang, D.Z., Mclnnes, B.I.A., Jiang, S.Y., Wang, R.C., Kanisawa, S., 2004. Two subgroups of A-type granites in the coastal area of Zhejiang and Fujian Provinces, SE China: age and geochemical constraints on their petrogenesis. Trans. Roy. Soc. Edin.: Earth Sci. 95, 227–236.

Qiu, J.S., Xiao, E., Hu, J., Xu, X.S., Jiang, S.Y., Li, Z., 2008. Petrogenesis of highly fractionated – type granites in the coastal area of northeastern Fujian Province: constraints from zircon U–Pb geochronology, geochemistry and Nd–Hf isotopes. Acta Petrol. Sinica 24 (11), 2468–2484 (in Chinese with English abstract).

Qiu, J.S., Li, Z., Liu, L., Zhao, J.L., 2012. Petrogenesis of the Zhangpu composite granite pluton in Fujian Province: constraints from zircon U–Pb ages, elements geochemistry and Nd–Hf isotopes. Acta Geol. Sinica 86 (4), 561–576 (in Chinese with English abstract).

Rajesh, H.M., 2000. Characterization and origin of a compositionally zoned aluminous A-type granite from South India. Geol. Mag. 137 (3), 291–318.

Rollinson, H.R., 1993. Using Geochemical Data: Evaluation, Presentation, Interpretation. Longman/Wyllie, Harlow/New York.

Shaw, D.W., 1970. Trace element fractionation during anatexis. Geochim. Cosmochim. Acta 34, 237–243.

Shaw, S.E., Flood, R.H., Pearson, N.J., 2011. The New England Batholith of eastern Australia: evidence of silicic magma mixing from zircon $^{176}Hf/^{177}Hf$ ratios. Lithos 126, 115–126.

Shen, W.Z., Zhu, J.C., Liu, C.S., Xu, S.J., Ling, H.F., 1993. Sm–Nd isotopic study of basement metamorphic rocks in south China and its constraint on material sources of granitoids. Acta Petrol. Sinica 9, 115–124 (in Chinese).

Shu, L.S., Yu, J.H., Wang, D.Z., 2000. Late Mesozoic granitic magmatism and its relation to metamorphism-ductile deformation in the Changle–Nan'ao fault zone, Fujian Province. Geol. J. China Univ. 6 (3), 368–378 (in Chinese with English abstract).

Skjerlie, K.P., Johnston, A.D., 1993. Fluid-absent melting behavior of an F-rich tonalitic genesis at mid-crustal pressures: implications for the generation of anorogenic granites. J. Petrol. 34, 785–815.

Söderlund, U., Patchett, P.J., Vervoort, J.D., Isachsen, C.E., 2004. The 176Lu decay constant determined by Lu–Hf and U–Pb isotope systematics of Precambrian mafic intrusions. Earth Planet. Sci. Lett. 219, 311–324.

Vervoort, J.D., Blichert-Toft, J., 1999. Evolution of the depleted mantle: Hf isotope evidence from juvenile rocks through time. Geochim. Cosmochim. Acta 63, 533–556.

Wei, C.S., Zhao, Z.F., Spicuzza, M.J., 2008. Zircon oxygen isotopic constraint on the sources of late Mesozoic A-type granites in eastern China. Chem. Geol. 250, 1–15.

Whalen, J.B., Currie, K.L., Chappell, B.W., 1987. A-type granites: geochemical characteristics, discrimination and petrogenesis. Contrib. Miner. Petrol. 95 (4), 407–419.

Whalen, J.B., Jenner, G.A., Longstaffe, F.J., Robert, F., Gariépy, C., 1996. Geochemical and isotopic (O, Nd, Pb and Sr) constraints on A-type granite petrogenesis based on the Topsails igneous suite, Newfoundland Appalachians. J. Petrol. 37, 1463–1489.

Wolf, M.B., London, D., 1994. Apatite dissolution into peraluminous haplogranitic melts: an experimental study of solubilities and mechanisms. Geochim. Cosmochim. Acta 58 (19), 4127–4245.

Wong, J., Sun, M., Xing, G.F., Li, X.H., Zhao, G.C., Wong, K., Yuan, C., Xia, X.P., Li, L.M., Wu, F.Y., 2009. Geochemical and zircon U–Pb and Hf isotopic study of the Baijuhuajian metaluminous A-type granite: extension at 125–100 Ma and its tectonic significance for South China. Lithos 289–305, 289–304.

Wright, J.B., 1969. A simple alkalinity ratio and its application to questions of nonorogenic granite genesis. Geol. Mag. 106 (4), 370–384.

Wu, F.Y., Sun, D.Y., Li, H.M., Jahn, B.M., Wilde, S., 2002. A-type granites in northeastern China: age and geochemical constraints on their petrogenesis. Chem. Geol. 234 (1–2), 105–126.

Xiao, E., Qiu, J.S., Xu, X.S., Jiang, S.Y., Hu, J., Li, Z., 2007. Geochronology and geochemistry of the Yaokeng alkaline granitic pluton in Zhejiang Province: petrogenetic and tectonic implications. Acta Petrol. Sinica 23 (6), 1431–1440 (in Chinese with English abstract).

Xu, X.S., Dong, C.W., Li, W.X., Zhou, X.M., 1999. Late Mesozoic intrusive complexes in the coastal area of Fujian SE China: the significance of the gabbro–diorite–granite association. Lithos 46, 299–315.

Xu, X.S., O'Reilly, S.Y., Griffin, W.L., Pearson, N.J., He, Z.Y., 2007. The crust of Cathaysia: age, assembly and reworking of two terranes. Precambr. Res. 158, 51–78.

Yang, J.H., Wu, F.Y., Chung, S.L., Wilde, S.A., Chu, M.F., 2006. A hybrid origin for the Qianshan A-type granite, northeast China: geochemical and Sr–Nd–Hf isotopic evidence. Lithos 89, 89–106.

Yang, Y.F., Yang, J.J., Li, N.M., Yan, Q., Zhan, X., Dong, C.W., 2010. SHRIMP U–Pb zircon dating of the basic-intermediate dikes from the coastland of Fujian Province. Geol. Sci. Technol. Inform. 29, 23–29 (in Chinese with English abstract).

Zhang, Z.J., Wang, Y.H., 2007. Crustal structure and contact relationship revealed from deep seismic sounding data in South China. Phys. Earth Planet. Inter. 165, 114–126.

Zhang, G.S., Wen, H.J., Hu, R.Z., Qiu, Y.Z., Xu, C., 2007. Genesis and dynamic setting of mafic dikes in southeastern Fujian: evidence from Sr–Nd isotopic and major and trace element geochemistry. Acta Petrol. Sinica 23 (4), 793–804 (in Chinese with English abstract).

Zhao, J.H., Hu, R.Z., Liu, S., 2004. Geochemistry, petrogenesis, and tectonic significance of Mesozoic mafic dikes, Fujian Province, southeastern China. Int. Geol. Rev. 46, 542–557.

Zhao, J.H., Hu, R.Z., Zhou, M.F., Liu, S., 2007. Elemental and Sr–Nd–Pb isotopic geochemistry of Mesozoic mafic intrusion in southern Fujian Province, SE China: implications for lithospheric mantle evolution. Geol. Mag. 144, 937–952.

Zhao, J.L., Qiu, J.S., Li, Z., Li, Y.L., 2012. Petrogenesis of the Taiwushan granite pluton in Fujian Province: constraints from zircon U–Pb ages and Hf isotopes. Acta Petrol. Sinica 28 (12), 3938–3950 (in Chinese with English abstract).

Zhou, J.C., Chen, R., 2001. Geochemistry of late Mesozoic interaction between crust and mantle in southeastern Fujian Province. Geochimica 30 (6), 547–558 (in Chinese with English abstract).

Zhou, X.R., Wu, K.L., 1994. Zhangzhou I- and A-type Complex. Science Press, Beijing (in Chinese with English abstract).

Zhou, J.C., Zhang, H.J., Yu, Y.W., 1994. Magma mixing in early Cretaceous composite lava flows in Xinchang, Zhejiang. Acta Petrol. Sinica 10 (3), 236–247 (in Chinese with English abstract).

Zhou, X.M., Sun, T., Shen, W.Z., Shu, L.S., Niu, Y.L., 2006. Petrogenesis of Mesozoic granitoids and volcanic rocks in South China: a response to tectonic evolution. Episodes 29, 26–33.